



SAE Aero Design East, 2022

School Name: Dwarkadas J. Sanghvi College of Engineering

Team Name: DJS SKYLARK - REGULAR CLASS

Team Number: 026

Team Members

Team Captain: Tanmay Kshire

Abhishek Malichkar
Aditya Bhalerao
Aditya Suri
Anushka Shah
Ardon Kotey
Arshish Balaporia
Arya Raut
Aryan Ashar
Deep Dholakia
Hariaksh Pandya

Harshal Soni
Het Shah
Hetavi Mehta
Joel Ponmany
Krish Morabiya
Malay Thumbar
Manthan Mistry
Mrunmay Mhapankar
Nimish Sabnis

Parv Khandelwal
Radhika Jethwa
Rayaan Juvale
Shlok Mandloi
Shubham Modi
Siddhi Tamanekar
Tejas Pathak
Vighnesh Patil

STATEMENT OF COMPLIANCE

Certification of Qualification

Team Name	DJS Skylark - Regular Class	Team Number	026
School	Dwarkadas J. Sanghvi College of Engineering		
Faculty Advisor	Prof. Shashikant Auti		
Faculty Advisor's Email	shashikant.auti@gmail.com		

Statement of Compliance

As faculty Adviser:

SMA (Initial) I certify that the registered team members are enrolled in collegiate courses.

SMA (Initial) I certify that this team has designed and constructed the radio-controlled aircraft in the past nine (9) months with the intention to use this aircraft in the 2022 SAE Aero Design competition, without direct assistance from professional engineers, R/C model experts, and/or related professionals.

SMA (Initial) I certify that this year's Design Report has original content written by members of this year's team.

SMA (Initial) I certify that all reused content have been properly referenced and is in compliance with the University's plagiarism and reuse policies.

SMA (Initial) I certify that the team has used the Aero Design inspection checklist to inspect their aircraft before arrival at Technical Inspection and that the team will present this completed checklist, signed by the Faculty Advisor or Team Captain, to the inspectors before Technical Inspection begins.



Signature of Faculty Advisor

04/04/2022

Date



Signature of Team Captain

4/4/2022

Date



Table of Contents

List of Figures, Tables, Symbols, and Abbreviations	2
1.0 Executive Summary	3
1.1 System Overview and Discriminators	3
1.2 Interpretation of Scoring Requirements	3
1.3 Competition Projections	4
2.0 Project Management	4
2.1 Schedule Summary	4
2.2 Personnel Management	5
2.3 Cost Report	5
2.4 Risk Analysis	6
3.0 Design Layout and Trades	6
3.1 Overall Design Features and Details	6
3.2 Competitive Scoring Strategy and Analysis	9
3.3 Design Derivations	12
3.4 Interfaces and Attachments	15
4.0 Loads, Environments and Assumptions	16
4.1 Design Load Derivations	16
4.2 Environmental Considerations	17
5.0 Analyses	17
5.1 Analytical Tools	17
5.2 Developed Models	18
5.3 Performance Analyses	19
5.3.1 Dynamic Thrust	19
5.3.2 Take-off and Climb-out Performance	19
5.3.3 Flight and Maneuver Performance	20
5.3.4 Static and Dynamic Stability	20
5.3.5 Payload Prediction Analysis	21
5.3.6 Drag Polar Analysis	21
5.4 Structural Analyses	21
5.4.1 Critical Margins	21
5.4.2 Applied Loads and Material Selection	22
6.0 Sub-Assembly Tests and Integration	24
6.1 Propulsion System and Testing	24
6.2 Battery and Servo Testing	24
6.3 Flight Testing	24
7.0 Manufacturing	25
8.0 Conclusion	25
Appendix A – Backup Calculations	26
Appendix B – Technical Data Sheet	
2D Drawing	



List of Abbreviations

CG	Center of Gravity	TMA	Tail Moment Arm
FoS	Factor of Safety	CAD	Computer Aided Drawing
MoS	Margin of Safety	CFD	Computational Fluid Dynamics
UTM	Universal Testing Machine	AR	Aspect Ratio

List of Symbols

C	Chord of Control Surface	S_{TO}	Take-off Distance
C_D	Drag Coefficient of Aircraft	T_d	Dynamic Thrust
C_{Di}	Lift-Induced Drag Coefficient	T_s	Static Thrust
C_{D0}	Zero-Lift Drag Coefficient	V	Airspeed
C_f	Skin Friction Drag Coefficient	V_d	Dive Speed of Aircraft
C_L	Lift Coefficient of Aircraft	V_E	Aircraft Equivalent Speed
C_M	Coefficient of Moment	V_{gE}	Gust Equivalent Speed
k_g	Gust Alleviation Factor	V_{Stall}	Stall Speed of Aircraft
L	Lift	V_{TO}	Velocity Require to Take-off
m	Mass of the Aircraft	V_x	Velocity of Aircraft in x-direction
n	Load Factor	V_y	Velocity of Aircraft in y-direction
n_{max}	Maximum Load Factor	α	Angle of Attack
S	Wing Planform Area	ρ	Density
S_1	Maximum Control Surface Deflection	ω	Frequency
S_2	Maximum Servomotor Deflection	ϕ	Aircraft Bank Angle

List of Figures and Tables

Figure 1(a)	System Overview and Discriminators	Figure 4(c)	Environmental Considerations
Table 1(b)	Subsystem Details	Chart 5(a)	Developed Models
Figure 2(a)	Schedule Summary	Figure 5(b)	Dynamic Thrust Performance
Figure 2(b)	Schedule and Cost Breakdown	Figure 5(c)	Take-off and Climb-out Telemetry
Table 2(c)	Risk Analysis	Table 5(d)	Post Flight-Test Optimization
Figure 3(a)	Wing Layout	Figure 5(e)	Minimum Turning Radius
Figure 3(b)	Fuselage Layout	Figure 5(f)	Maximum Banking Angle
Figure 3(c)	Empennage Layout	Table 5(g)	Stability Response
Figure 3(d)	Electronics System Layout	Figure 5(h)	Phugoid and Short Period Modes
Figure 3(e)	Planform Analysis	Table 5(i)	Lateral Stability Eigenvalues
Figure 3(f)	Cargo Configuration Analysis	Figure 5(j)	Drag Polar Analysis
Figure 3(g)	Overall Scoring Strategy	Table 5(k)	Material Selection
Table 3(h)	Trial Prototype Configuration Selection	Figure 5(l)	Crosswind Analysis
Figure 3(i)	High Lift Devices	Figure 5(m)	Composite Stress Analysis
Figure 3(j)	C_M vs Alpha	Figure 5(n)	Weight Buildup
Figure 3(k)	Motor-Propeller Combinations	Figure 6(a)	Novel Wind Tunnel Setup
Figure 4(a)	V-n Diagram	Table 6(b)	Servo Torque Requirements
Table 4(b)	Landing Shock Calculations	Chart 7(a)	Manufacturing Process

1.0 Executive Summary

1.1 System Overview and Discriminators

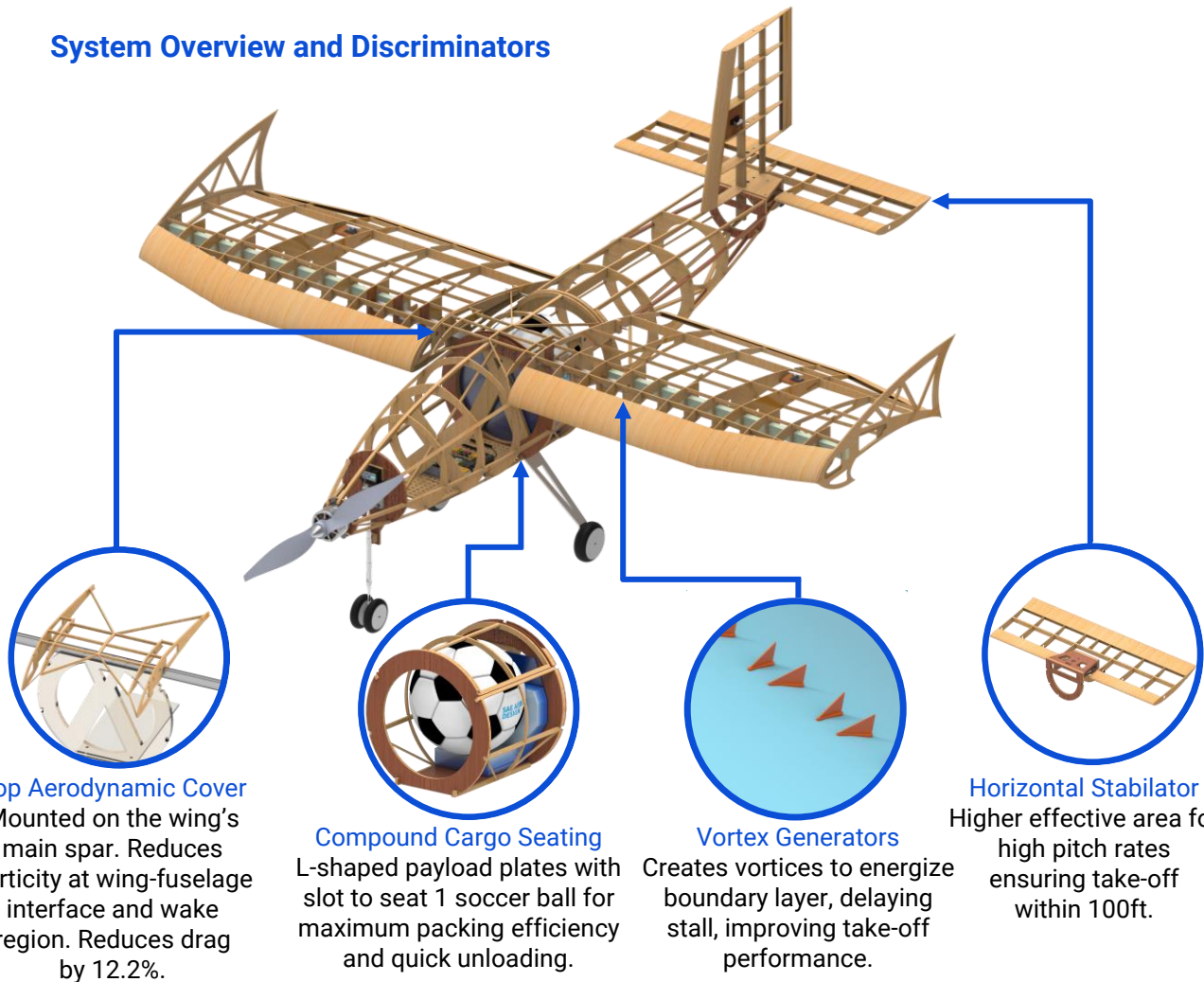


Figure 1(a): System Overview and Discriminators

Avionics	Motor	Propeller		Battery
	SunnySky X5320-12 250Kv	APC 21x12WE		Tattu Lipo 3300mAh 6S
Wing	Airfoil	Span	Aspect Ratio	Planform
	S1223RTL	70 in.	3.03	Recto-Trapezoidal
Empennage	Vertical Tail Airfoil	Horizontal Tail Airfoil		Configuration
	NACA-0009	AH 79-100C (75%) – NACA-0009 (25%) interpolated		Inverted T-Tail
Scoring Strategy	Cargo Configuration	Cargo Bay Length	Spherical Cargo	Boxed Cargo Lifted
	One Ball Compound Cargo	9 in.	1 Soccer Ball	17.265 lbs.

Table 1(b): Subsystem Details

1.2 Interpretation of Scoring Requirements

To maximize the score, the team attempted to understand its sensitivities to each parameter of the scoring equation. We identified fuselage drag, propulsion system selection, and crosswind performance as other key areas of development to optimize performance and maximize score.



1.3 Competition Projections

The team designed the aircraft to carry 18.140 lbs. of total cargo weight, comprising 1 Soccer Ball and 17.265 lbs. of Boxed Cargo; achieving a projected score of 30.782 points per round and 102.346 points in total including the Payload Prediction Bonus. Combining our flight scores with strong Design Report and Technical Presentation scores, we aim to place in the Top 3 Overall. This predicted flight score has been obtained by performing an in-depth analysis on the scoring equation to understand which parameters to optimize, followed by extensive trade studies for each component based on the results obtained from the former.

2.0 Project Management

2.1 Schedule Summary

The COVID-19 pandemic and the resulting curfews in India heavily affected the team's schedule throughout the year. The team began work in September as the restrictions were relaxed until when, we trained recruits and researched different designs and ideas. We based our timeline on cycles of design, testing, and optimization, working around our exam schedule. We built four trial prototypes, empirically testing design and scoring philosophies. Three development prototypes were built upon the selected philosophy. With each, we introduced a slew of improvements which saw an increase in score and scoring consistency (**Section 5.3.2**).

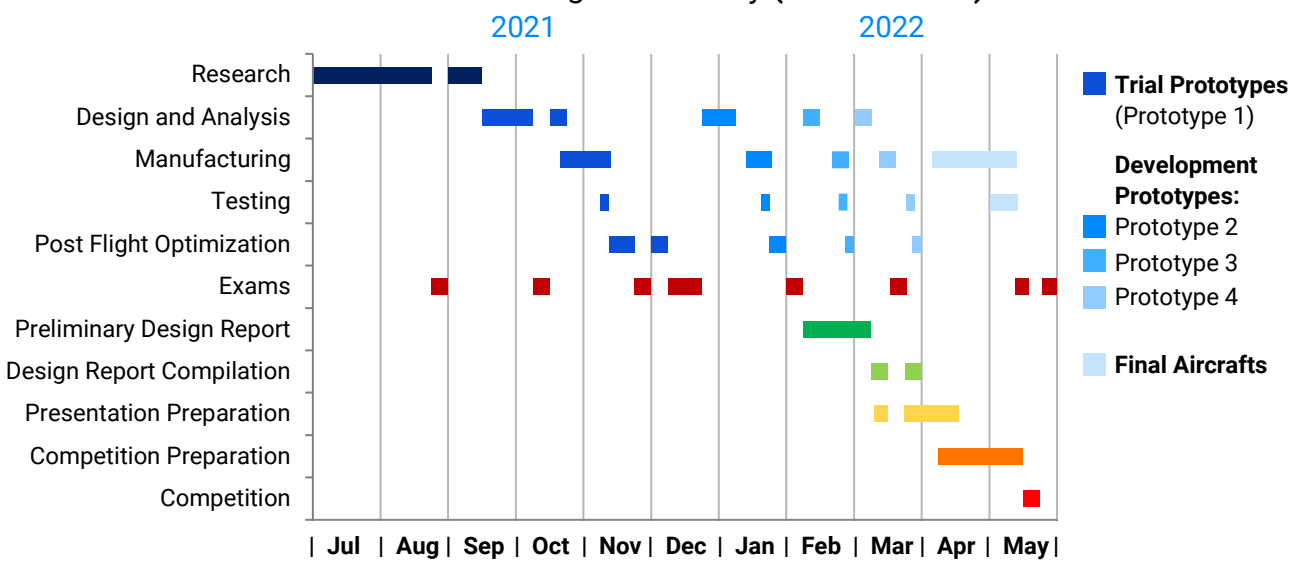


Figure 2(a): Schedule Summary

2.2 Personnel Management

Comprising of 28 students, the team was segregated into aerodynamics, structures and stability, avionics, and marketing departments. This ensured that ideas could be shared and discussed effectively inter and intra-departmentally allowing for the efficient execution of the schedule mentioned above. Over time, the Design Report and Technical Presentation groups were formed.

2.3 Cost Report

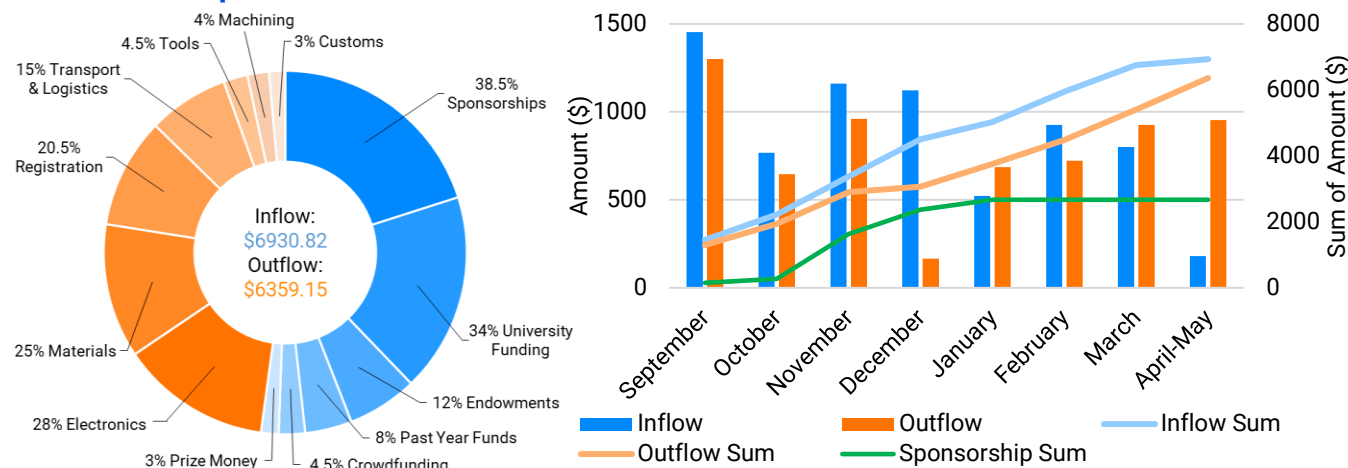


Figure 2(b): Schedule and Cost Breakdown

COVID-19 heavily affected the team's inflow of funds, starting with delayed university funding, reduced crowdfunding, and cancellation of the annual aero-modeling workshop that the team conducts to raise funds. The outflow of funds largely comprised of electronic components, raw material procurement, registration fee, tools, and logistics. To reduce the high material procurement costs, we contacted international wholesalers directly. We also used electronics and materials from past years in the trial prototype phase to reduce spending. High customs duties, long shipping periods, and product unavailability worldwide limited our options for testing electronics, which we overcame by using online tools to shortlist components. Certain radical designs, such as biplanes, could not be extensively tested due to a constant high requirement of manpower, which was limited due to COVID-19 restrictions. Having to build 2 sets of wings per prototype and high customs duties on additional electronics would have compounded our financial burden. Figure 2(b) represents how funds were managed throughout the year.



2.4 Risk Analysis

Risk Factor	Mitigation	Outcome
COVID - 19 Pandemic	Team vaccination; Frequent RT-PCR tests; Stagger members for manufacturing; Double masking; Workshop sanitization.	26/28 members COVID negative over the year; 92.85% negativity rate.
Structural Component Failure	Use high tensile strength materials (Figure 5(m)); Assemble structures with strong bonding agents and cyanoacrylates.	Increased structural reliability and reduced failure rate to 1/11 flight rounds.
Material Acquisition Delays	Use materials & components sparingly; Order materials in timely cycles; Wholesale Orders	Material available in urgency; No delays in manufacturing; Lowered Costs
Monetary Constraints	Sponsorships; Crowd funding; Acquire funds through member contributions. (Section 2.3)	Spare funds for emergencies; Ensured uninterrupted operations of the team.
High Impact Landing Shocks	Used custom made Aluminum main landing gear with a sweep angle and nose landing gear with telescopic suspension. (Section 4.1.2)	All impulsive loads absorbed by the landing gears; No baseplate failure in 10/10 full payload flight rounds.
Wing & Tail Strikes	Addition of wingtip fence & tapered fuselage tail to ensure ground clearance for the tail.	Assisted in reducing weight of the wing by 20% and 14.5% of tail.
Crosswinds & Gusts	Minimize longitudinal section area; Optimize rudder performance (Section 5.4.2)	Smoothen flight trajectory; Immediate corrections to adverse yaw motions.
Servo & Control Surface Failures	Endurance testing performed on servos.	No flight crashes due to servo failures.

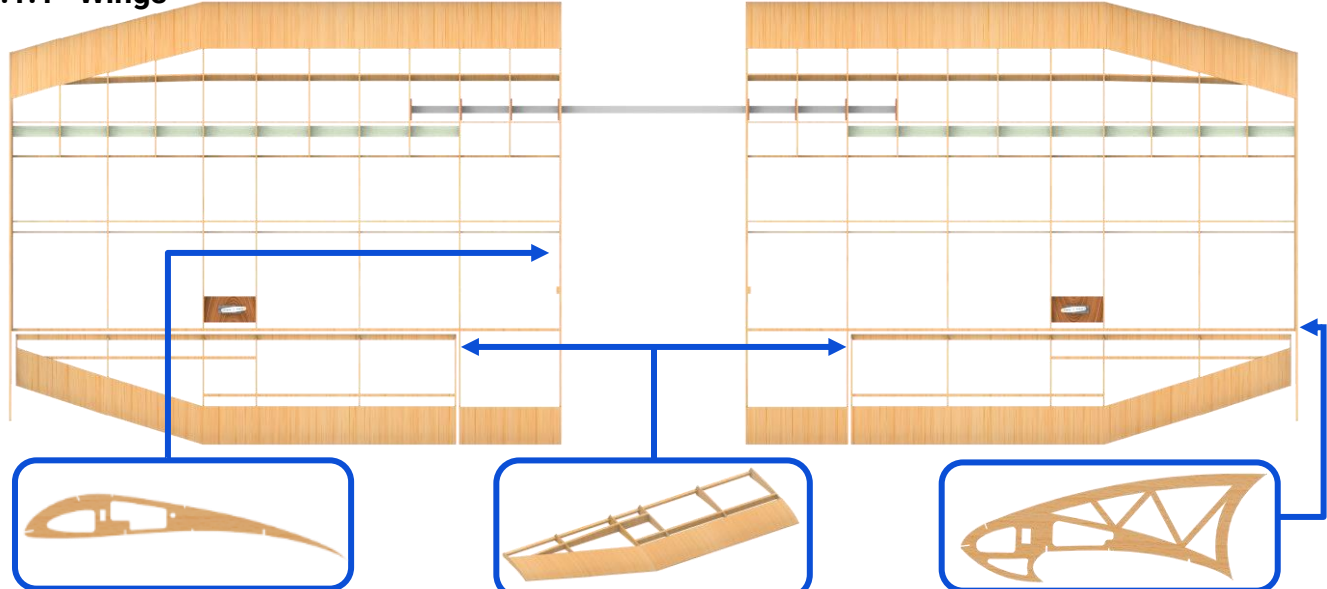
● Impact (High/Medium)

Table 2(c): Risk Analysis and Mitigation

3.0 Design Layout and Trades

3.1 Overall Design Features and Details

3.1.1 Wings



Airfoil Shaped Ribs
S1223RTL with 24" root chord and 18" tip chord used. Weight reductions implemented.

Flaperons
Reduces take-off distance; Covers 15.58% of wing area, provides high rolling moments & high lift due to propwash.

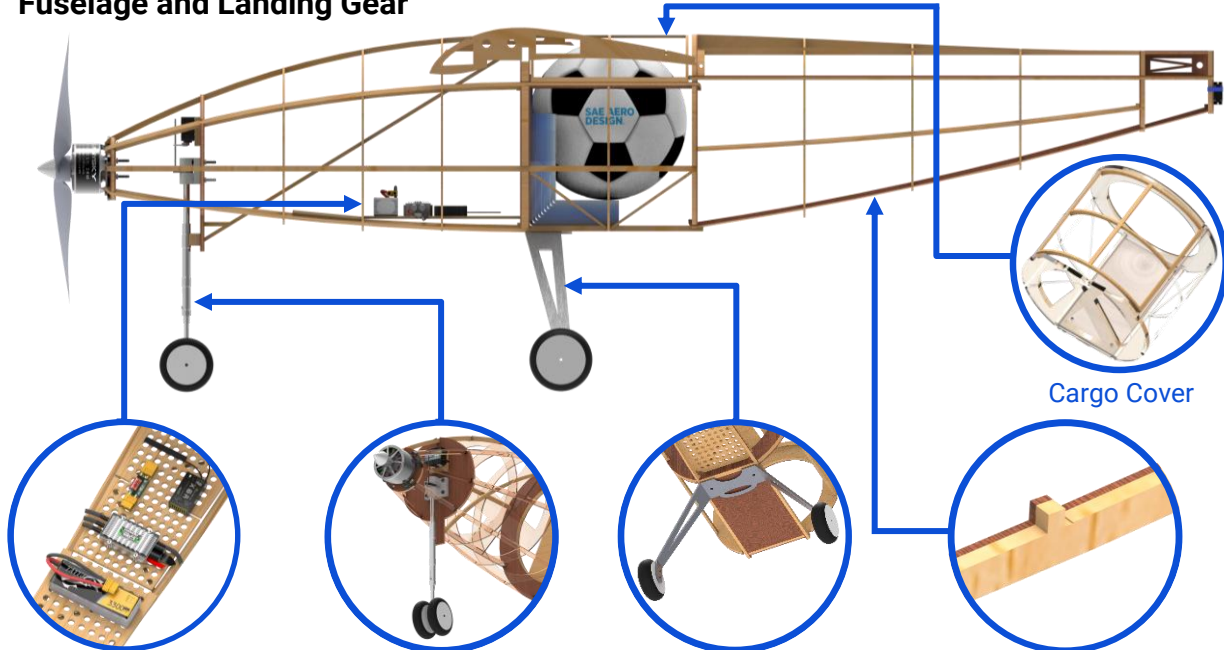
Wingtip-Fence Winglet
Decreases intensity of vortices and increases lift by 5.88%. The fence protects from wing-strikes and reduces winglet height by delaying leakage of high-pressure air.

Figure 3 (a): Wing Layout

The team opted for a recto-trapezoidal planform where the rectangular section provides comparatively high lift within the region affected by propwash. The tapered section has

substantially lesser induced drag and assists in achieving the velocities required for take-off. The wing is made of airfoil-shaped ribs, retained in place with balsa jigs. A main spar with hollow aluminum in the center and XPS foam to the sides is used to sustain in-flight loads within MoS, while maintaining a low empty weight.

3.1.2 Fuselage and Landing Gear



Avionics Bay

Perforated structure in the nose section to secure electronic components safely and allow easy access to repair or replace them.

Landing Gear

Aluminum Main Landing Gear implemented to sustain landing shocks. Nose Landing Gear mounted on strut to prevent buckling and ensure safety during ground run.

Composite Structure

Laminates of basswood ply and balsa used to reinforce longerons, baseplate and bulkheads.

Figure 3(b): Fuselage Layout

We designed the fuselage as a chassis structure comprising three sections: the nose, mid, and tail sections; for ease of manufacturing. The tail section tapered from the side at an angle of 6.4° and the aerodynamic cover present at the wing-fuselage interface produces a streamlined structure to promote laminar airflow to the stabilator, also reducing drag by 33.31%. We designed a smaller circular firewall instead of a larger rectangular one, reducing form drag by 15.5%, and empty weight by 22.22%. A tricycle landing gear is used owing to its immunity to ground looping. The Main Landing Gear, designed using topology optimization, has an aluminum structure to resist landing impacts (**Section 4.1.2**) and reduce empty weight. The aluminum Nose Landing Gear has a spring-loaded suspension to absorb impacts and protect the nose.



3.1.3 Boxed and Spherical Cargo

As per Section 1.3, we decided to go for a 1-ball strategy with 17.265 lbs. of boxed payload in the form of L-shaped mild steel plates. The spherical cargo was placed inside a circular slot of the payload plates (**Figure 1(a)**) ensuring its proximity to the overall CG. This arrangement along with the cargo cover formed the Compound Cargo Bay, restricting the movement of the ball in all axes. The cargo cover facilitated unloading in 35 seconds, and loading in under 2 minutes, reducing turnaround time to allow frequent flight rounds in the newly introduced Round-less system. Efficient packaging, ease of loading, and machinability of steel plates were given priority, their dimensions being derived primarily from the dimensions of the ball.

3.1.4 Empennage

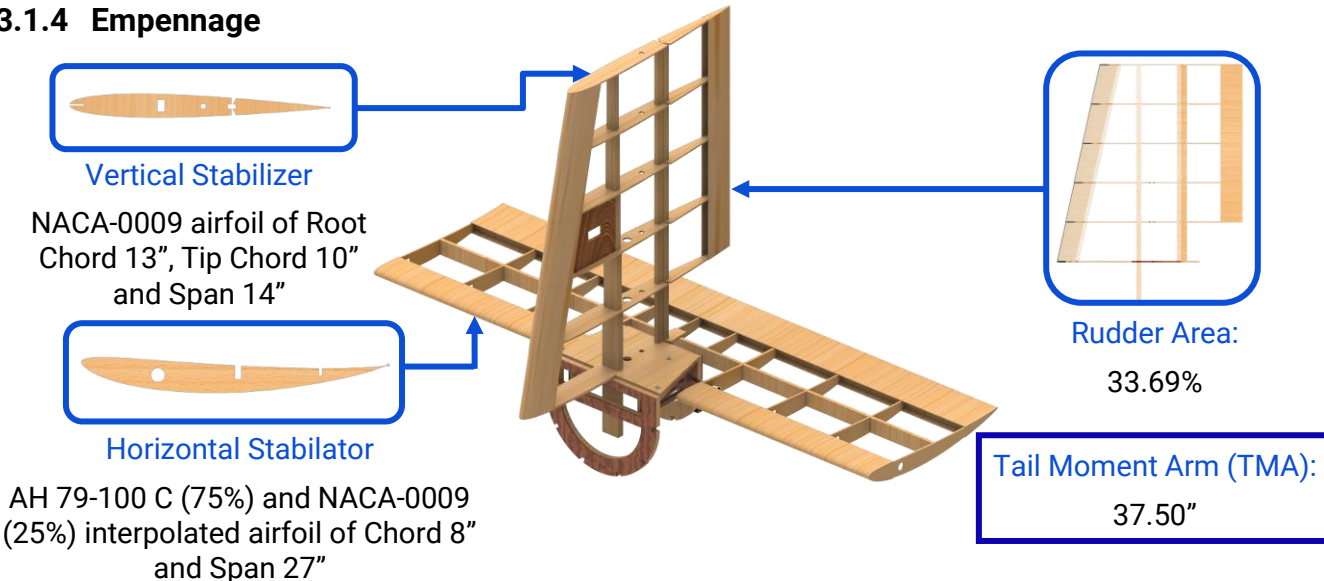


Figure 3(c): Empennage Layout

The aircraft utilizes an inverted T-Tail configuration for its reliability while reducing empty weight by 45% compared to a U-Tail. We decided to use a stabilator instead of a conventional elevator arrangement to provide higher pitching moments (**Section 3.3.4**). A staggered primary spar was used for the vertical stabilizer, progressively widening from the top to bottom to provide structural reinforcement at the base. Rudder effectiveness was ensured in crosswind conditions (**Figure 5(l)**) through appropriate stabilizer sizing (**Section 3.3.3**) and laminar airflow to the empennage due to the addition of aerodynamic covers.

3.1.5 Avionics

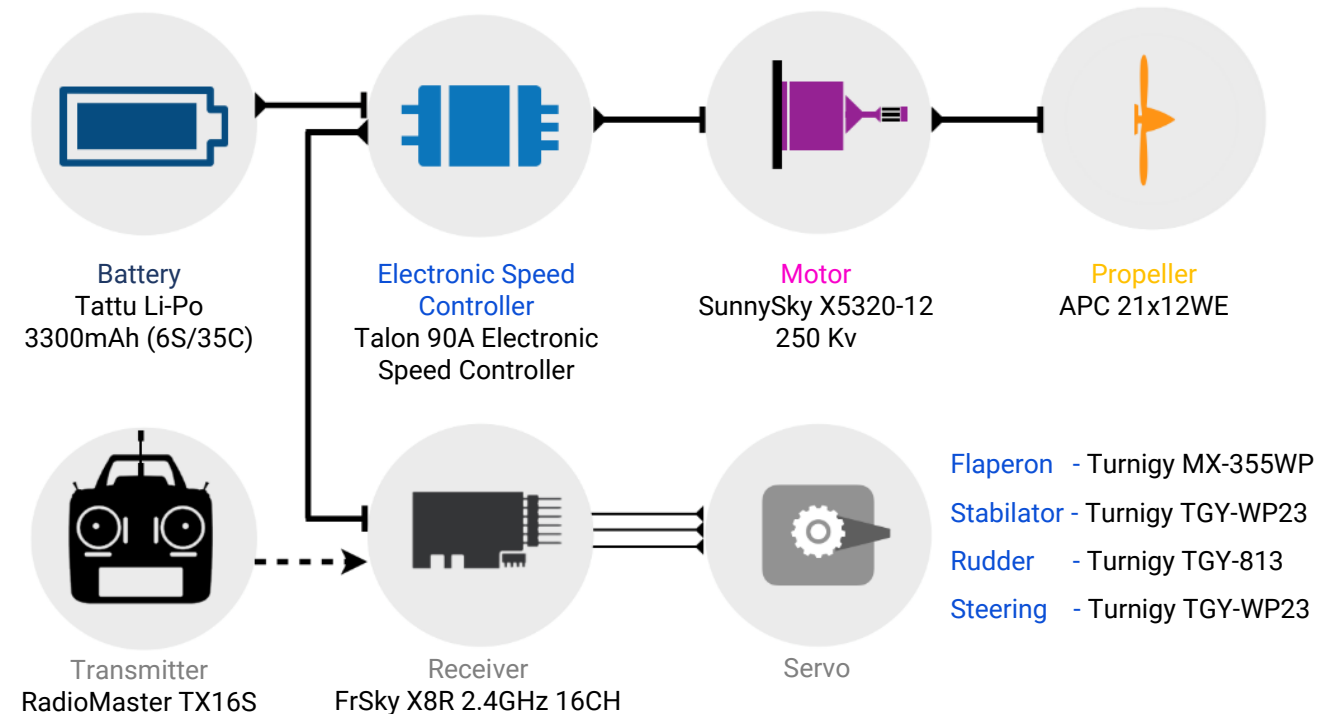


Figure 3(d): Electronics System Layout

3.2 Competitive Scoring Strategy and Analysis

The optimization goal of the scoring equation is to maximize the numerator, i.e., number of balls and payload, and to minimize the denominator, i.e., span and cargo bay length. In order to accomplish this while keeping in mind the 100ft. takeoff distance and 1000W power limit, we performed an exhaustive search in the domain (**Chart 5(a)**) to find the optimal wing planform and cargo configurations. As the planform and cargo configurations are independent of each other, it is possible to optimize them individually, and combine their effects to obtain the overall scoring strategy. The top four configurations were tested empirically (Trial Prototypes) in varying conditions to achieve the mean score and finalize the configuration and strategy.

3.2.1 Planform Analysis

We performed an exhaustive search of airfoils which focused on maximizing lift, airfoil efficiency, and stall angle, while minimizing drag and shortlisted S1223RTL, CH10 and E420. These were then analyzed in Tornado VLM Solver in MATLAB on over 5500 wing planforms with varying dimensions as shown in Section 5.2. From this we inferred that S1223RTL performed

better, averaging 5.13% and 4.5% more points as compared to E420 and CH10, respectively, when tested in our scoring and take-off distance mathematical model (**Section 5.2**). Further, the top 10% scoring configurations of each span were shortlisted, and high-mesh CFD Analyses (**Section 5.1.1**) were run for more accurate results. We factored in the empty weight increase for spans by calculating the quantity of balsawood and adhesives used, evaluating mass properties provided by our CADs and past manufactured weights. Lift and Drag values obtained were used as inputs to our mathematical model. Simulations on biplanes exhibited a 38% lift increase, but weight of reinforcements negated the lift obtained due to manufacturing limitations. Moreover, manpower, cost and logistical constraints also influenced the decision to discard the same.

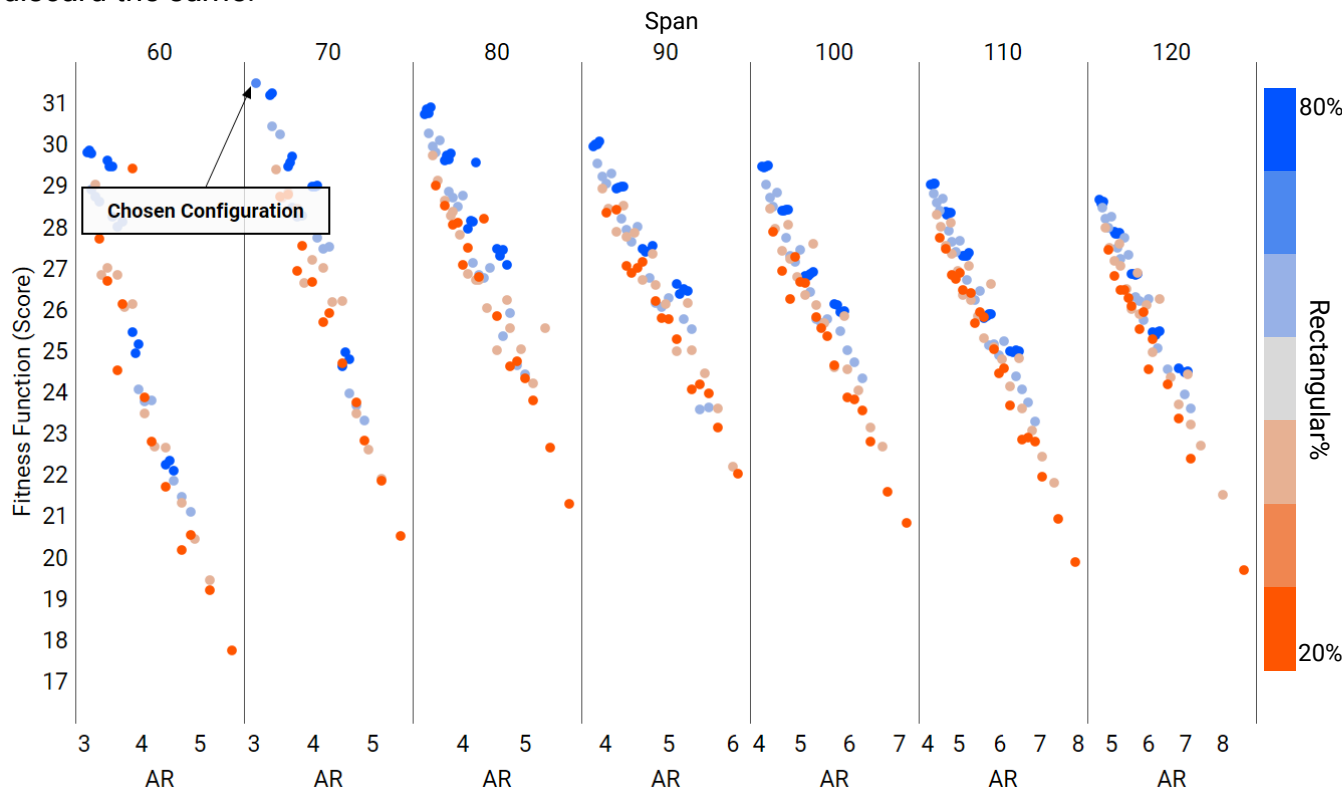


Figure 3(e): Planform Analysis

As cargo configuration was kept constant, we could compare performance effectively. Scores have been plotted above with each of the 550 data points representing various planforms. Lower aspect ratios and higher rectangular percentages with spans ranging from 70-90" have the best scoring characteristics owing to higher lift despite increased drag. Hence, we chose to maximize

all-up weight lifted, compromising on drag, to reduce the span penalty on the scoring equation.

The final planform selected has a Span of 70", Root and Tip Chord 24" and 18", Rectangular % of 70%, Angle of Incidence 5° and an AR of 3.030.

3.2.2 Cargo Configuration Analysis

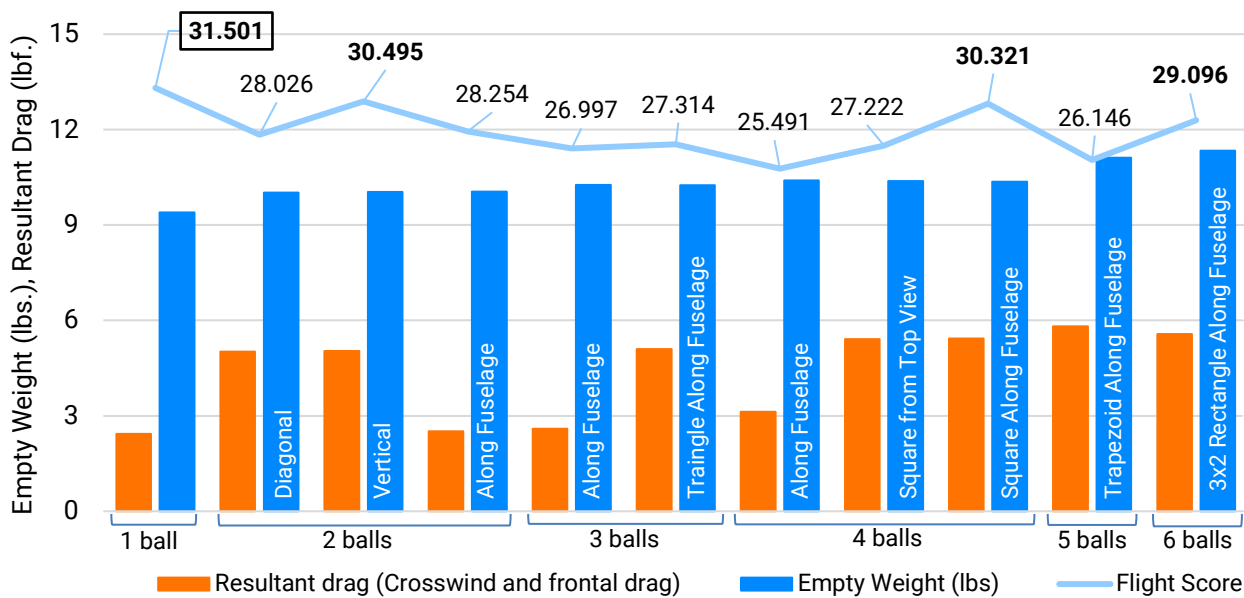


Figure 3(f): Cargo Configuration Analysis

To shortlist cargo configurations, the team calculated scores for each fuselage and ball configuration keeping the wing planform constant, plotting them against their respective crosswind performance and empty weights (derived from CADs; scaled down test sections). All 3 ball & 5 ball configurations are filtered out for their inefficient use of cargo bay length and negligible drag reduction. We shortlisted 1 ball, 2 ball vertical, 4 ball square along fuselage and 6 ball rectangle configurations to be tested, on the basis of score obtained from the analysis.

3.2.3 Overall Scoring Strategy and Configuration Selection

The team divided the scoring strategy into Planform and Cargo Configuration Analysis. While varying one, the other was kept constant, allowing for direct comparisons. The wing planform lifting the highest all-up weight within 100ft. was chosen, regardless of cargo layout. Figure 3(g) shows the scores of each planform with shortlisted cargo configurations from Section 3.2.2 against span to find optimal span for each configuration.

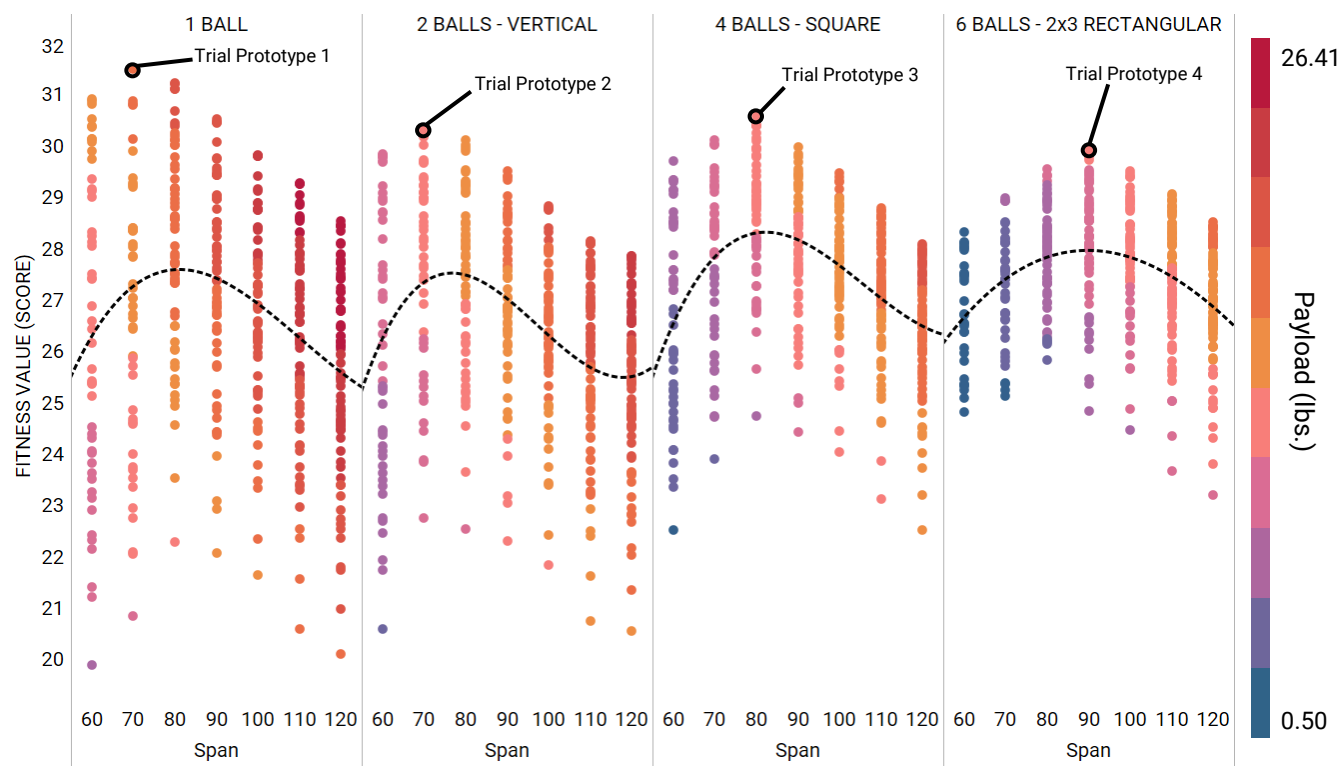


Figure 3(g): Overall Scoring Strategy

We selected the global maxima of each configuration and manufactured these aircraft configurations (using experiential data for 4 ball square configuration) using optimal motor-propeller combinations for each configuration. We found the mean scores of 10 best flight rounds of each configuration in varying conditions. From these results, we finalized the 1-ball configuration, as the development prototype, for its consistent score in all conditions.

Trial Proto No.	Optimal Motor-Propeller	Mean Score	Reason for Elimination/Selection
Prototype - 1	SunnySky X5320-12 250Kv, 21X12WE	28.101	Aerodynamic structure, good crosswind performance, low empty weight
Prototype - 2	SunnySky X5320-12 250Kv, 22X10WE	26.582	Large wake region, poor crosswind performance and dynamically unstable
Prototype - 3	SunnySky X5320-12 250Kv, 22X12WE	27.245	High frontal drag & poor crosswind performance
Prototype - 4	Scorpion SII-5535 160Kv, 27x13E	26.154	Difficulties in reaching V_{TO} due high profile drag and empty weight

Table 3(h): Trial Prototype Configuration Selection

3.3 Design Derivations

3.3.1 Wings

The team built 4 prototypes, testing high-lift devices, weight reductions, and mountings. The first wing was devoid of any high-lift devices to obtain a performance baseline. As the design progressed, we tested winglets, vortex generators and flaperons, which increased score, delayed

stall, and reduced drag. The high FoS of the first wing was reduced with each iteration; replacing the outer half of the aluminum spar with XPS foam, adding half-airfoil ribs and spars to retain shape while reducing weight. We chose the high wing mount over low and mid, to primarily have a feasible compromise between ground effect, wing area affected by propwash and stability. A low wing mount was primarily discarded to avoid major wing strikes.

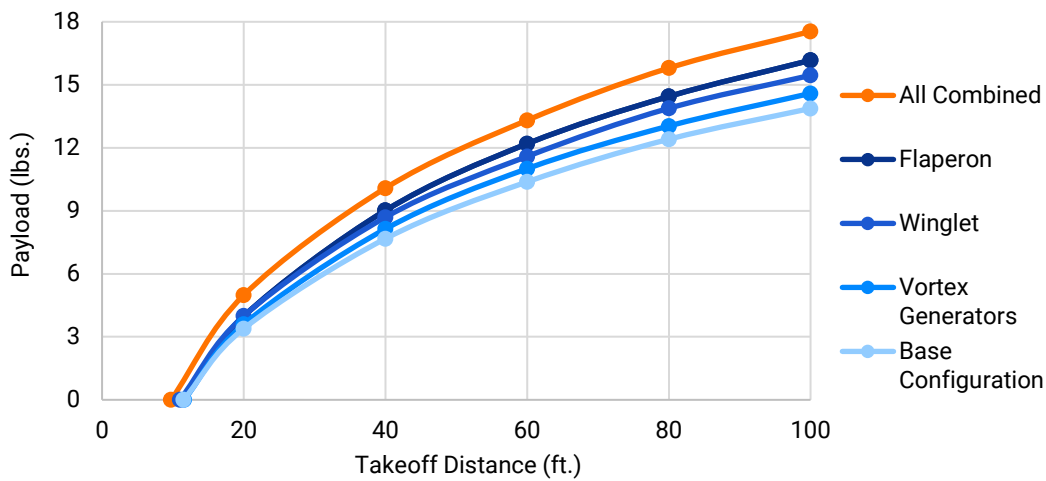


Figure 3(i): High Lift Devices

3.3.2 Fuselage and Landing Gears

The primary fuselage dimensions were derived by satisfying the required TMA, CG position, electronics, and payload bay capacities. UTM tests were performed to check the FoS of structural components [Section 5.4.2 2)]. The modularity of the nose-longerons was increased by 34.5%, reducing nose section weight by 0.15 lbs. We changed the cross-section of the firewall from a larger rectangular area to a smaller circular one as it distributed forces effectively to the longerons within MoS. The main landing gear (MLG) sweep angle of 8.9° was calculated on its free body diagram. This provided optimum strength to transmit normal reaction force and handle frictional force torque without causing undue stress on baseplate. The custom-made aluminum MLG provided precise control over CG calculations, and optimum propeller clearance.

3.3.3 Vertical Tail (VT)

The requirements for yawing were 33% lower than first calculated after extensive flight testing, due to a fuselage with small longitudinal section. Thus, we chose a conventional tail design



discarding U-tail and T-tail for their high empty weight and overcompensated yaw performance. We sized the tail by computing the required tail volume coefficient (0.04), analyzing crosswinds at Fort Worth (**Figure 5(l)**). NACA-0009 was selected for its low drag at 0° angle of attack.

3.3.4 Horizontal Tail (HT)

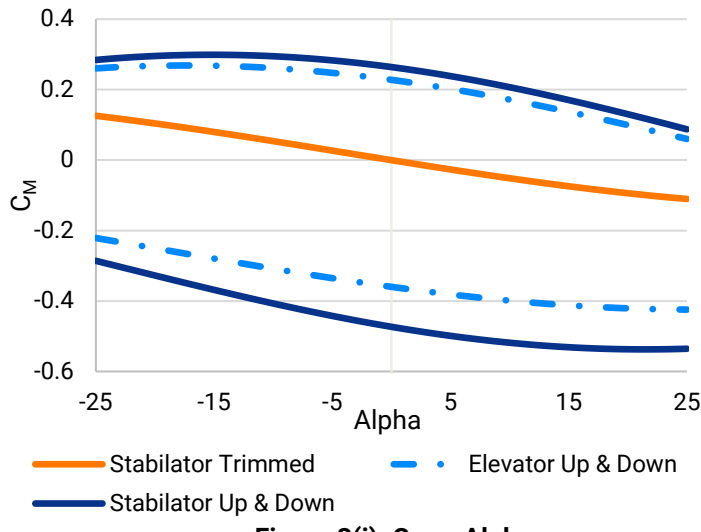


Figure 3(j): C_M vs α

The goal was to achieve positively stable empty and loaded CG positions, so the team calculated the resulting moments of each force acting on the aircraft. A stabilator with an inverted airfoil of 75% AH 79-100 C airfoil interpolated with 25% NACA-0009 airfoil was chosen to achieve

the required level of pitching moment and negative slope for C_M versus Angle of Attack.

3.3.5 Avionics

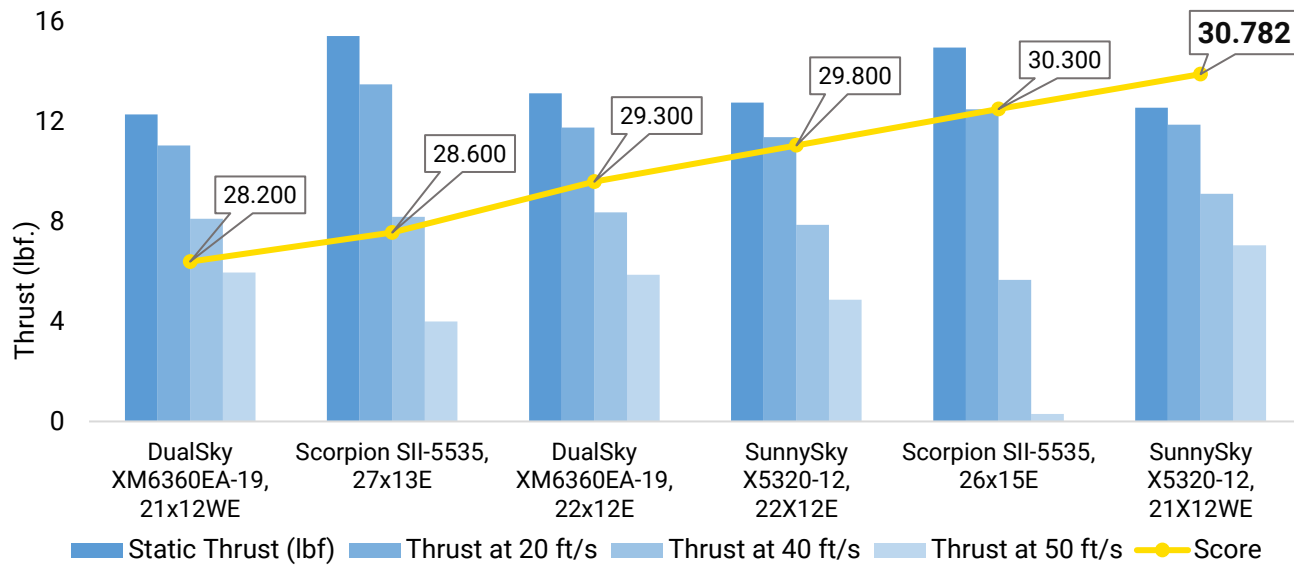
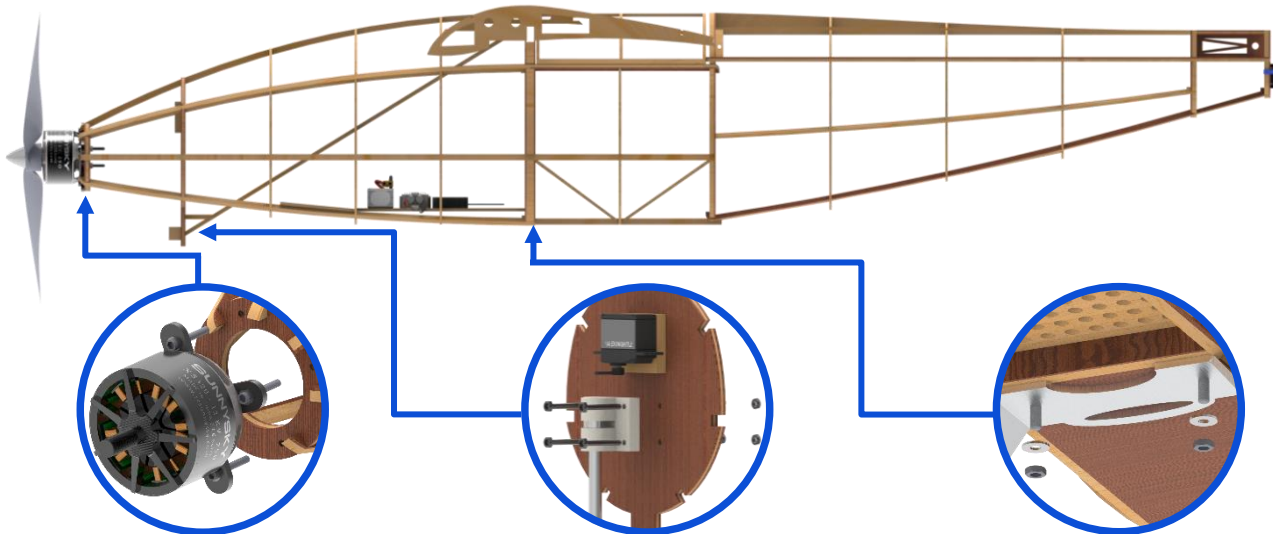


Figure 3(k): Motor-Propeller Combinations

The selection of motor-propeller was based on dynamic performance analysis (**Section 6.1**) for the flight conditions of take-off, turning and cruising. We chose SunnySky X5320-12 due to its exceptional dynamic performance and lower weight, in contrast to the Scorpion's higher static thrust but poor dynamic performance and higher weight.

3.4 Interfaces and Attachments



Motor Mounting

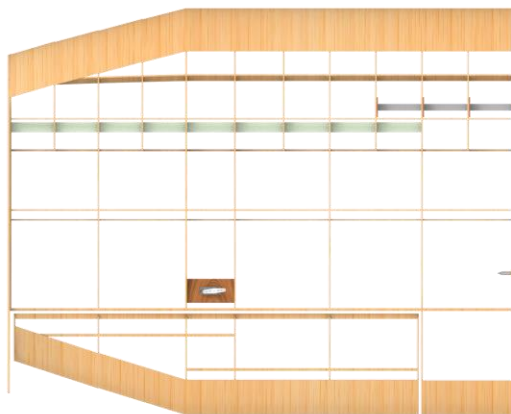
The firewall, made from laminate of basswood ply and balsa core, is used to attach the motor to the fuselage.

Nose Landing Gear Mounting

A Polyoxymethylene bush mounted on a modular plate is used to attach the nose landing gear to a thick laminate rib.

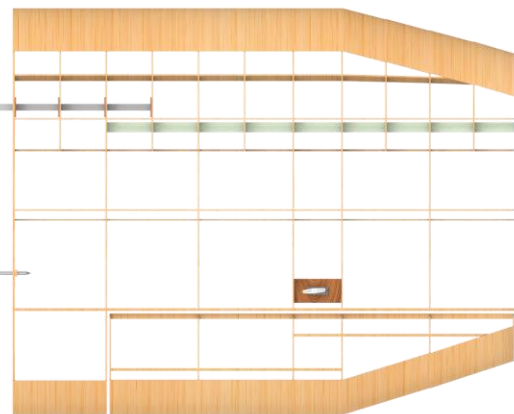
Main Landing Gear Mounting

Landing gear bolted to a thick composite baseplate in the cargo bay section of the fuselage.



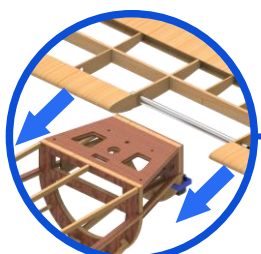
Primary Spar Locking

Bolting through co-axial holes in plywood formers of the mid-section on aligning with the primary spar.



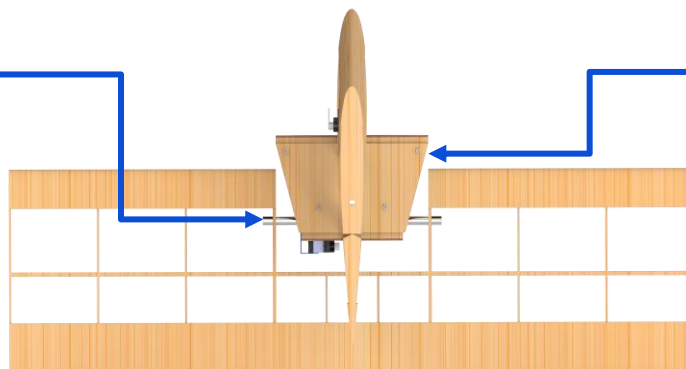
Rear Pin Locking

Stainless-steel spoke (pin) is used to connect tail bulkhead to the rear end of the wing.



Horizontal Stabilizer Mounting

Mounted using cylindrical main spar entering from the side through holes present at aft end of tail plate.



Vertical Stabilizer Mounting

Mounted on the top of the tail plate, using bolts.

4.0 Loads, Environment and Assumptions

4.1 Design Load Derivations

4.1.1 V-n Diagram

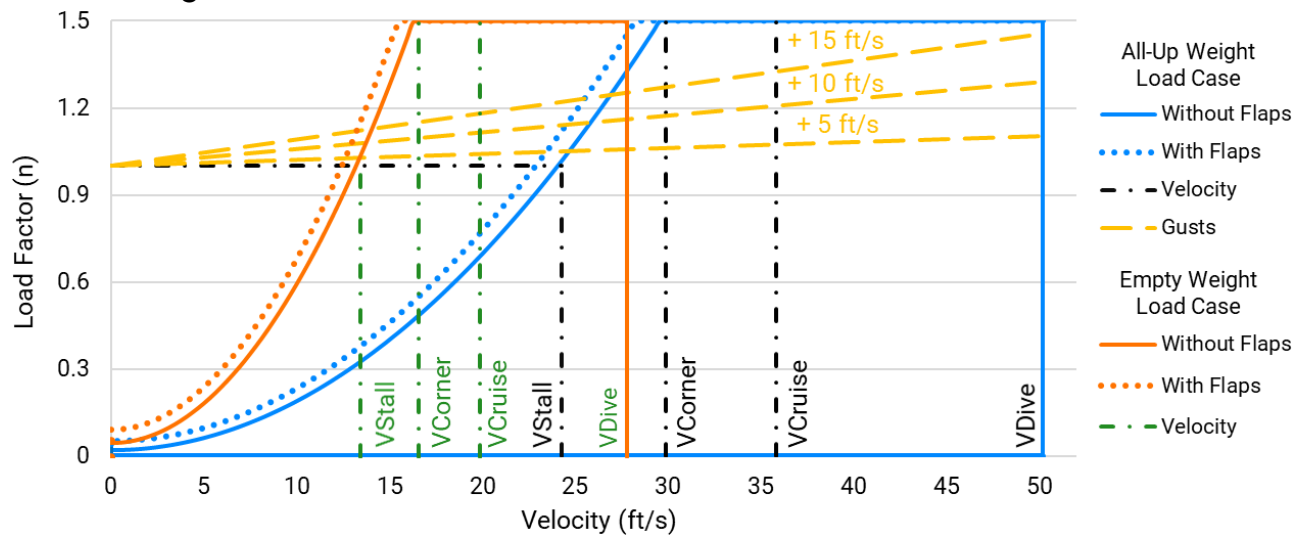


Figure 4(a): V-n Diagram

The V-n diagram is generated for empty and all-up weight of the aircraft. The load factor is nonzero when the aircraft is stationary because of propwash. Flap deployment extends the flight envelope of the aircraft, as can be seen by the dotted lines. Gust velocities of 5ft/s, 10ft/s and 15ft/s were also considered for the all-up weight load case.

4.1.2 Landing Shocks

Sink Angle	Sink Rate	Impact Loading (lbf.)
3°	1.49576227	222.8685782
5°	2.490912193	371.1459167
8°	3.977568919	592.6577689

Table 4(b): Landing Shock Calculation

The team calculated the impact loading on the airframe during touchdown for sink angle of 3°, 5° and 8° by calculating change in momentum and normal force. We used telemetry data to derive the former and calculate approach velocity. We recorded the median impact time as 0.2 seconds from multiple flight tests. We used a custom-made aluminum landing gear (Figure 3(b)) over carbon fiber, reducing weight and FoS, capable of sustaining impact loads mentioned above. The fuselage baseplate and landing gear was designed with a FoS of 1.51 and 1.6, respectively, keeping these loads in mind.

4.2 Environmental Considerations

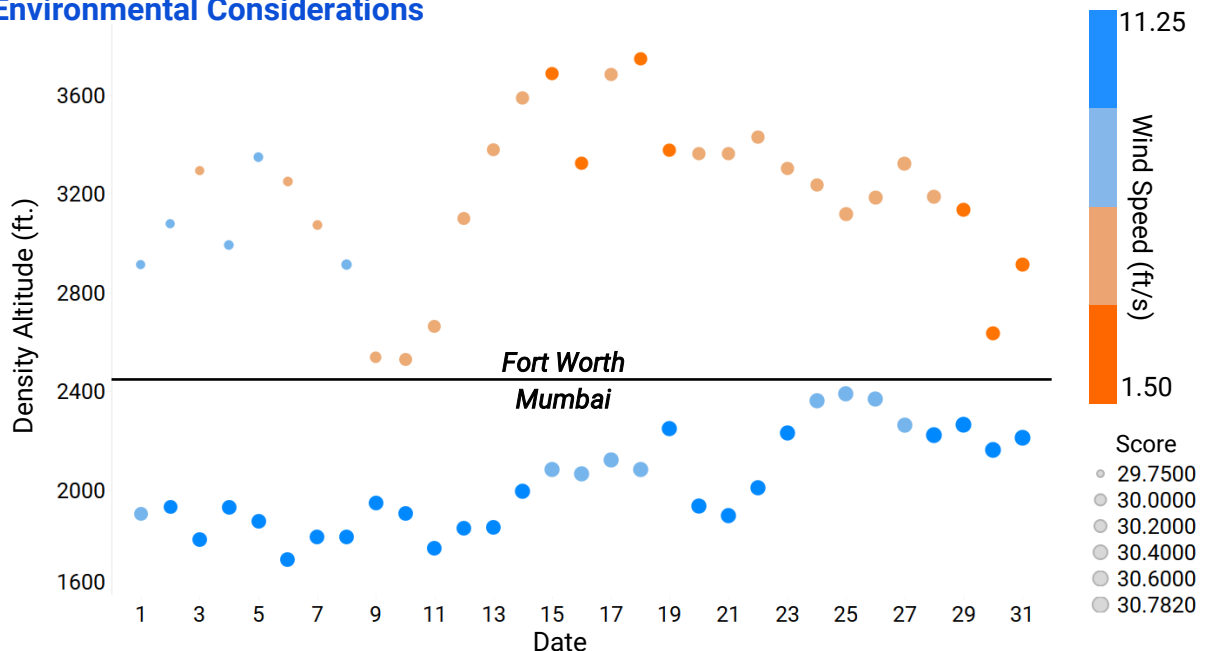


Figure 4(c): Environmental Considerations

We calculated the scores for the months of March and May for Mumbai and Fort Worth respectively. This was derived from their density altitudes, taking into account various environmental factors using historical data of temperature, pressure, relative humidity, dew point, and altitude during the days of the competition as well as our testing period. We also took into account differing values of rolling resistance at these locations. The highest score obtained at Fort Worth is 30.444 points, with a decrease in score of 1.098% as compared to Mumbai.

5.0 Analyses

5.1 Analytical Tools

5.1.1 ANSYS & SolidWorks

The team used SolidWorks to perform low-mesh CFD to find the local maxima, whereafter ANSYS Fluent provided results on shortlisted planforms using a high element quality mesh to find the global maxima. ANSYS Mechanical was used for Finite Element Analysis (FEA) on load-bearing components. Topology Optimization and Response Surface techniques on ANSYS were used to reduce the weight of structures, while varying several geometric parameters, but still lying within the MoS. SolidWorks was also used for high accuracy balancing of masses and CG.



5.1.2 XFLR5 & MATLAB

We used XFLR5 to interpolate airfoils and export their polars. It was also used for obtaining and analyzing static and dynamic stability eigenvalues (**Section 5.3.4**). Tornado VLM in MATLAB was used for analyses of airfoils to obtain C_L and C_D values. The Global Optimization Toolbox by MathWorks was used to optimize the above system variables using the advanced technique of genetic optimization to find the global maxima with the score being the fitness function.

5.1.3 Tableau & Microsoft Excel

They were used to generate detailed graphs, helping infer inter-variable relationships, that are otherwise abstruse. This visual representation aided in the development of the scoring strategy.

5.2 Developed Models

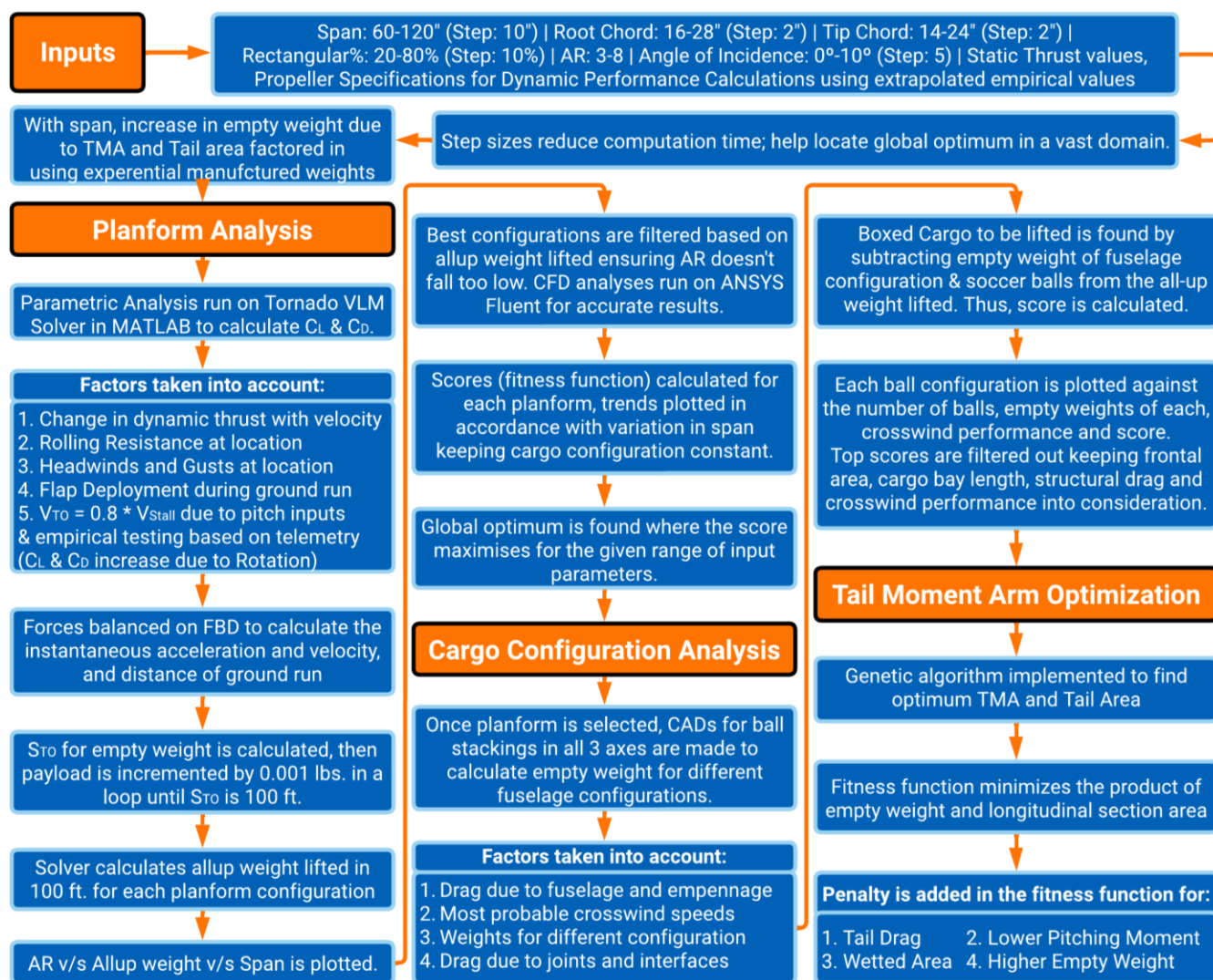


Chart 5(a): Developed Models



5.3 Performance Analyses

5.3.1 Dynamic Thrust Performance

We analyzed dynamic thrust characteristics of various motor-propeller combinations (**Section 3.3.5**) using the wind tunnel setup as described in **Section 6.0**. Figure 5(b) compares the values of the three best combinations identified through the above process, depicting payload vs take-off distance. Dynamic thrust was prioritized over static thrust allowing for flight in intense winds.

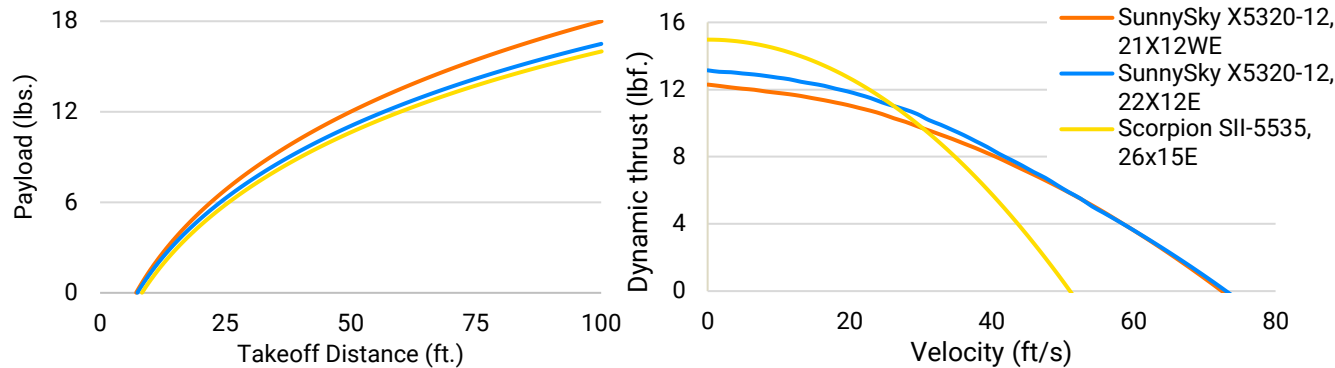


Figure 5(b): Dynamic Thrust Performance

5.3.2 Take-Off and Climb Out Performance

We incorporated equations governing take-off in our model (**Section 5.2**), running simulations for each development prototype. Below are the flight trajectories of our prototypes derived from telemetry obtained after empirical testing along with a progress summary.

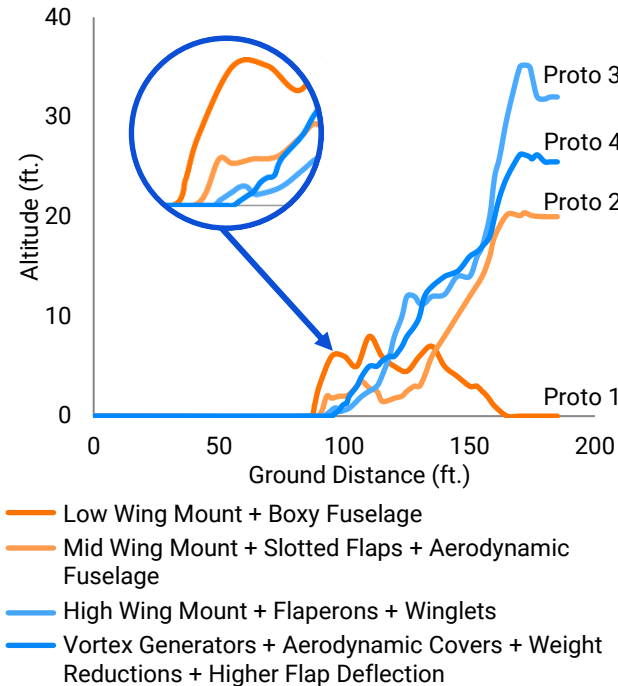


Figure 5(c): Take-off and Climb-out Telemetry

Prototype (Score)	Pros	Cons	To improve
1 (28.101)	Lifted payload of 15.5lbs. assisted by high ground effect.	Low velocity – high drag; Unstable; Wing strikes	Make fuselage aerodynamic, increase stability.
2 (28.557)	Lifted payload of 15.8lbs. Higher velocity achieved.	Distinct flaps led to weight increase. High pitching moment required.	Optimize TMA & tail size to balance moments about CG. Reduce drag due to flaps.
3 (29.620)	Lifted payload of 16.5lbs. as high lift due to flaperons. Stable flight.	High empty weight & FoS. Redundant structures.	Perform weight reductions, reduce wing and fuselage wake
4 (30.782)	Lifted target 17.265lbs. Stable flight.	Unable to lift any more, no take-off at 17.5 lbs. payload.	Final configuration set to 17.265lbs. payload plates & 1 ball as the top scoring flight.

Table 5(d): Post Flight-Test Optimizations

5.3.3 Flight and Maneuver Performance

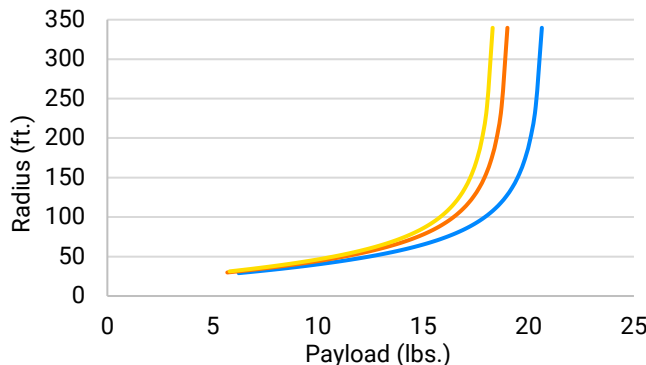


Figure 5(e): Minimum Turning Radius

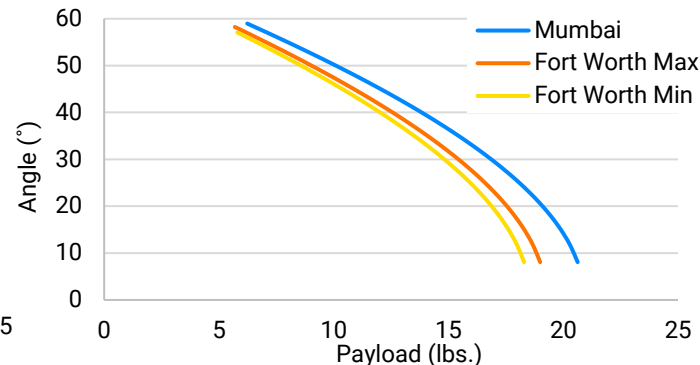


Figure 5(f): Maximum Banking Angle

The team calculated the maximum banking angles and turning radii for various load factors and velocities by resolving the forces acting on the free-body diagram of the aircraft at the maximum corner velocity (**Section 4.1.1**) for the locations' respective density altitudes.

5.3.4 Static and Dynamic Stability

The negative slope of C_M vs Angle of Attack (**Figure 3(j)**) indicates that the aircraft is statically stable. The neutral point is 24.37" from the aircraft datum and the static margin is 4.57% of Mean Aerodynamic Chord.

Oscillating Aircraft Dynamic Response		
Aircraft motion	Damping Factor	Oscillation Time (seconds)
Short Period (Longitudinal)	0.579	0.935
Phugoid (Longitudinal)	0.061	7.813
Dutch Roll (Lateral)	0.429	0.998
Non-oscillating Aircraft Dynamic Response		
Roll Dampening (Lateral)	Tau: 0.016	Dampening Time: 0.011 seconds
Spiral Instability (Lateral)	Pilot Response Time: 1.8 seconds	Pitch at Response Time: 120.5971 °/s

Table 5(g): Stability Response

Dynamic stability was assured by using analyses and empirical testing in varying conditions. We ensured FoS of 1.2 on all control surfaces allowing for the aircraft to be controllable in all axes.

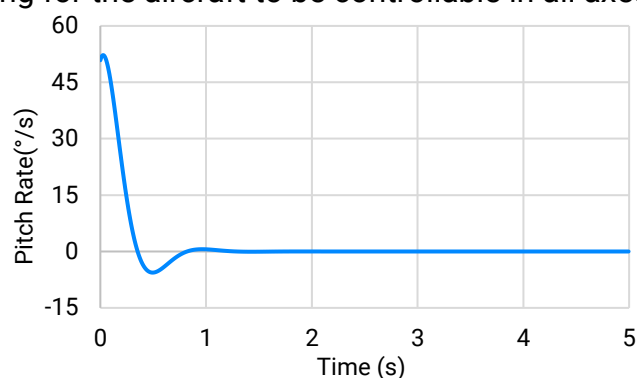
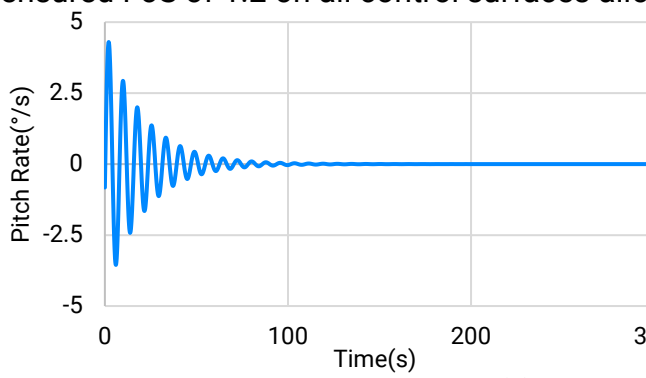


Figure 5(h): Phugoid and Short Period Modes



Roll Dampening	-63.51893	Dutch Roll	-2.72318+6.00236i	Spiral Instability	0.51163
----------------	-----------	------------	-------------------	--------------------	---------

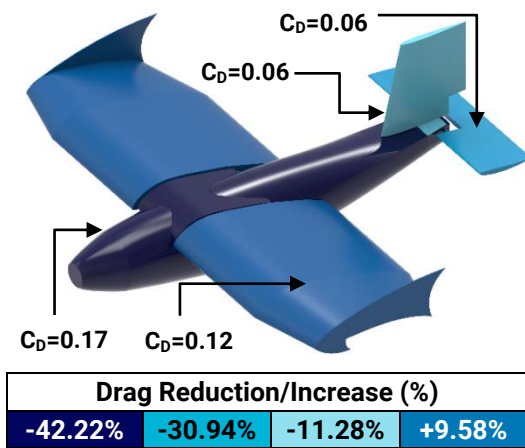
Table 5(i): Lateral Stability Eigenvalues

5.3.5 Payload Prediction Analysis

The payload lifted at different density-altitudes (DA) was calculated by the following formulae:

All-up weight lifted = L ; $L = (1/2) \cdot CL \cdot \rho \cdot S \cdot v^2$; $P = L - 9.4$; where P is the payload lifted. We created a DA calculator which, at standard conditions, outputs the ideal pressure and temperature, and consequently the density at different altitudes. The ambient weather conditions at our test site in Mumbai were recorded, and the DA was calculated. The value of the base all-up weight lifted at a DA of 0 ft. was then reverse engineered. Furthermore, we extrapolated the data in a range of 0 to 10000 ft. to find the all-up and the payload that could be lifted at all DAs. The equation of the line plotted from this data is: $y = -0.00075585x + 19.50208175$.

5.3.6 Drag Polar Analysis



The team calculated the percentage drag contributions of major components of the aircraft over the prototypes. A significant decrease in drag of the fuselage was obtained over iterations. An increase in the wing area led to an increase in drag. The net reduction in drag over all prototypes was 35.4%.

Figure 5(j): Drag Polar Analysis

5.4 Structural Analyses

5.4.1 Critical Margins

Material	Component/Condition	Max Stress Induced (PSI)	Max Allowed Stress (PSI)	FoS
Balsa	Stringers	1745	1914.5	1.097
Basswood	Baseplate during cruise	1994	2264.3	1.136
	Baseplate while turning	2193.4	2264.3	1.032
Aluminum	Wing Dowel during cruise	18860	26933.5	1.428
	Wing Dowel while turning	19803	26933.5	1.360
XPS Foam	Wing Insert during cruise	313.1	690.0	2.204
Mild Steel	Wing Locking during cruise	34192.62	53664	1.569
	Wing Locking while turning	35371.2	53664	1.517

Table 5(k): Material Selection

5.4.2 Applied Loads and Material Selection

1) Tail Force Analysis

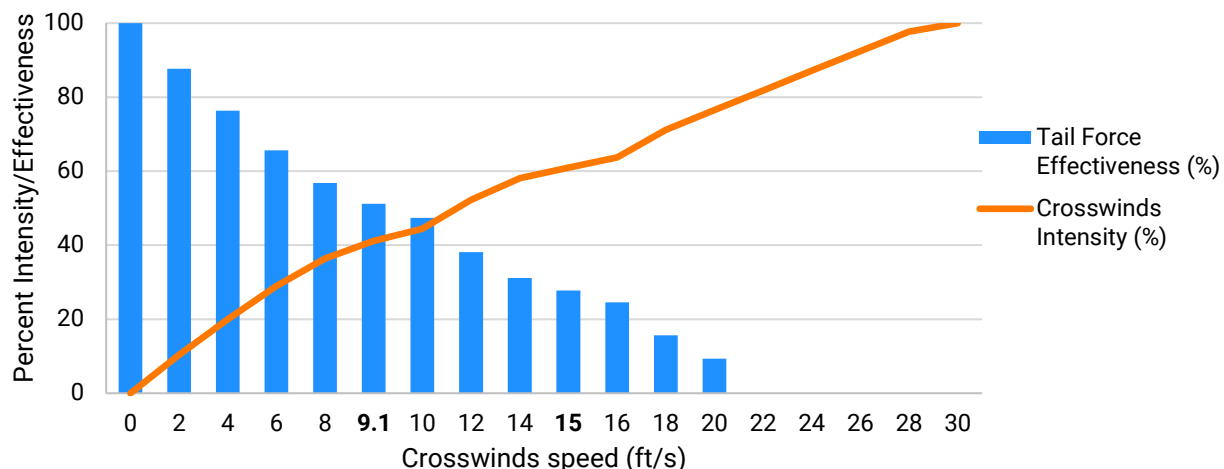


Figure 5(l): Crosswind Analysis

The team analyzed rudder effectiveness in crosswind conditions by developing a mathematical model where rudder forces were measured at varying crosswind intensities for in-flight conditions. The rudder becomes ineffective at crosswind velocity of 22.0 ft/s. Since Fort Worth has maximum wind speeds and gusts of 9.1 ft/s and 15.0 ft/s, according to past data, rudder performs at 51.22% and 27.77% effectiveness, respectively.

2) Material Selection

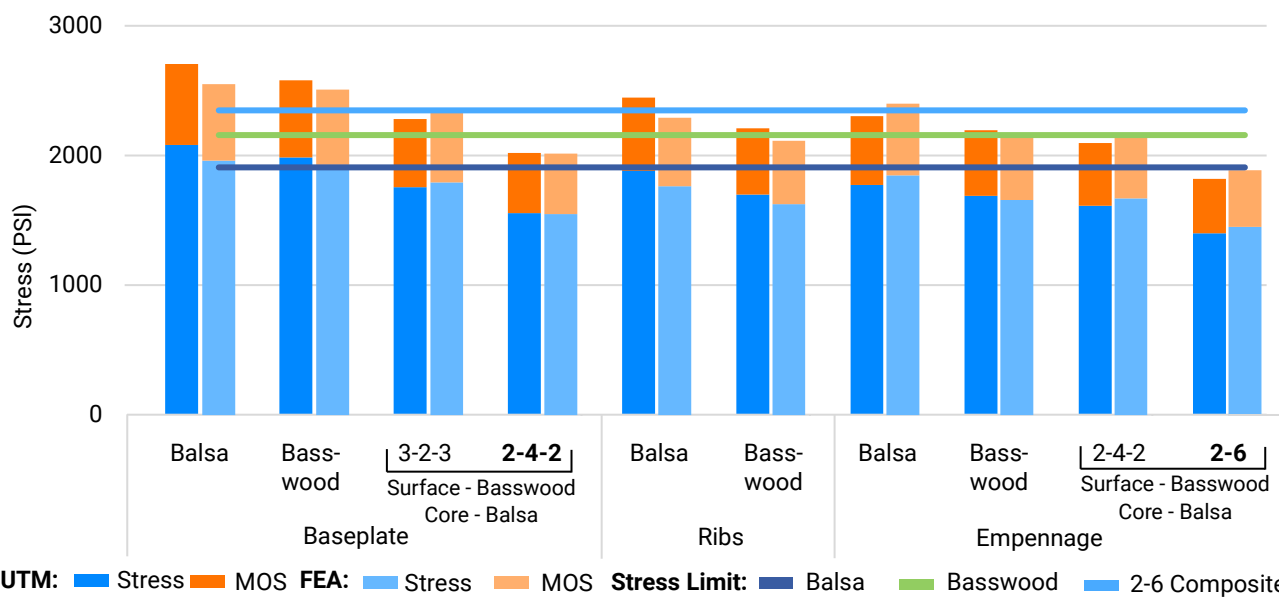


Figure 5(m): Composite Stress Analysis

We constructed the airframe primarily with wood, with the main wing spar made of a hollow rectangular cross-section aluminum beam for 37.97% of the span from the center line, and XPS

foam in the rest. This is attributed to aluminum's anisotropic strength, high endurance, greater resistance to shear and bending forces, and foam's immense strength to weight (S/W) Ratio. We used balsa in the wing and tail sub-assemblies for its low density and high S/W ratio. Laminates of balsa-basswood were used for the ribs, baseplate and longerons for having higher strength than balsa, strengthening critical areas while being lighter than conventional hardwood. Components were analyzed using Finite Element Analysis (FEA) and further tested on UTM to find their MoS and stress limits to reduce empty weight and FoS iteratively (**Figure 5(k)**). Based on these results, we used a basswood-balsa composite of 2-6 mm instead of 2-4-2 mm basswood-balsa-basswood, for longerons and tail bulkhead, reducing FoS from 1.43 to 1.28.

3) Mass Properties and Balance

A. Center of Gravity

Based on our calculations and pilot inputs, the aircraft was designed with the CG 1.01" in front of the Neutral Point ensuring static stability. The main landing gear was placed near the CG to achieve equal weight distribution and also prevent excessive loading on the nose landing gear.

B. Weight Distribution

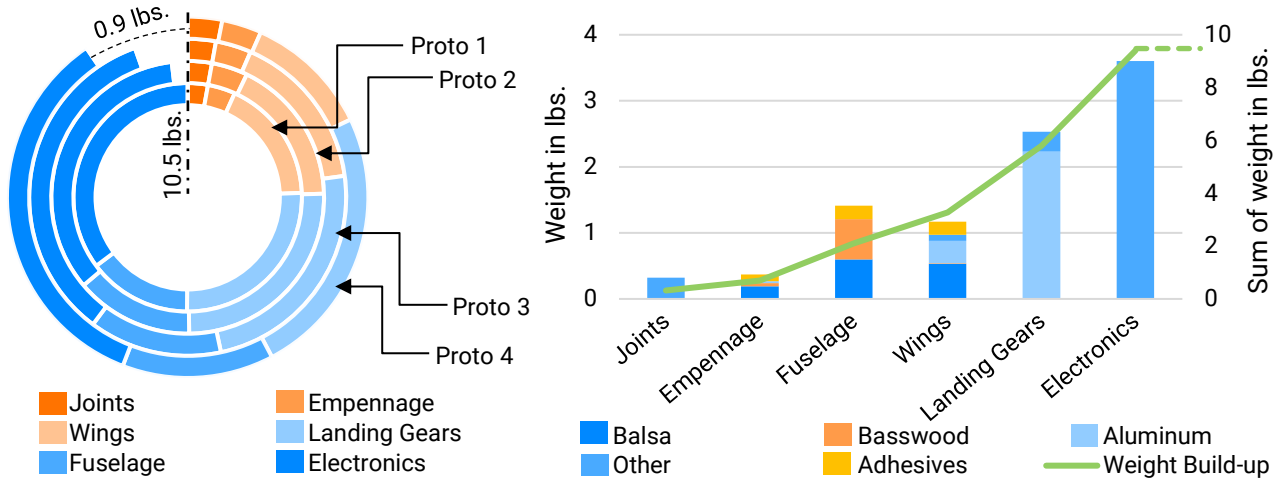


Figure 5(n): Weight Buildup

To minimize empty weight, each component was weighed before assembly. Weight reduction techniques were performed on components with lesser critical loading while reinforcing regions requiring a higher FoS. Empty weight was reduced with each iteration, as illustrated.

6.0 Sub-Assembly Tests and Integration

6.1 Propulsion System and Testing

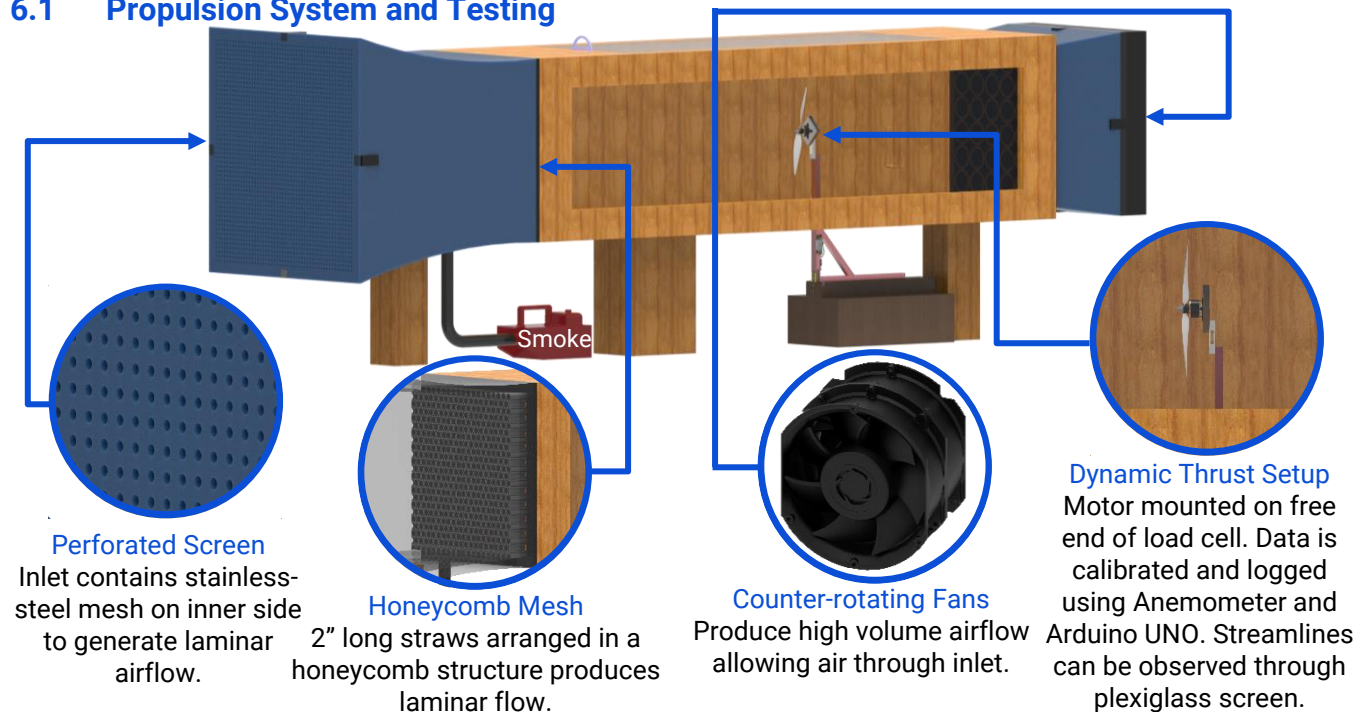


Figure 6(a): Novel Wind Tunnel Setup

The team shortlisted motor-propeller combinations after comparing thrust values from eCalc, limiting them to 1000W. We measured dynamic thrust using a wind tunnel (**Figure 6(a)**) having counter rotating fans at the outlet, and a honeycomb mesh & stainless-steel mesh in the contraction cone. We used a smoke system to view flow trajectories through plexiglass. The median error for thrust values was found to be 3.12%, when we compared to online tools.

6.2 Battery and Servo Testing

Battery endurance was tested by operating the motor statically at full throttle for the time taken to complete 2 flight rounds. We verified these results during flight tests for the same scenario.

Control Surface	Servomotor	Rated Torque (oz-in)	Control Surface Deflection	Required Torque (oz-in)
Flaperon	Turnigy MX-355WP	166.648	30°	60.775
Stabilator	Turnigy TGY-WP23	319.409	30°	116.38
Rudder	Turnigy TGY-813	124.986	30°	27.83
Nose Landing Gear (Steering)	Turnigy TGY-WP23	319.409	30°	250.17

Table 6(b): Servo Torque Requirements

6.3 Flight Testing

We tested various design configurations equipped with RPM and GPS sensors, accelerometer,



pitot tube and altimeter to gather telemetry data. We conducted flights with an incremental weight build-up strategy and compared analytical values with post-flight empirical values.

7.0 Manufacturing

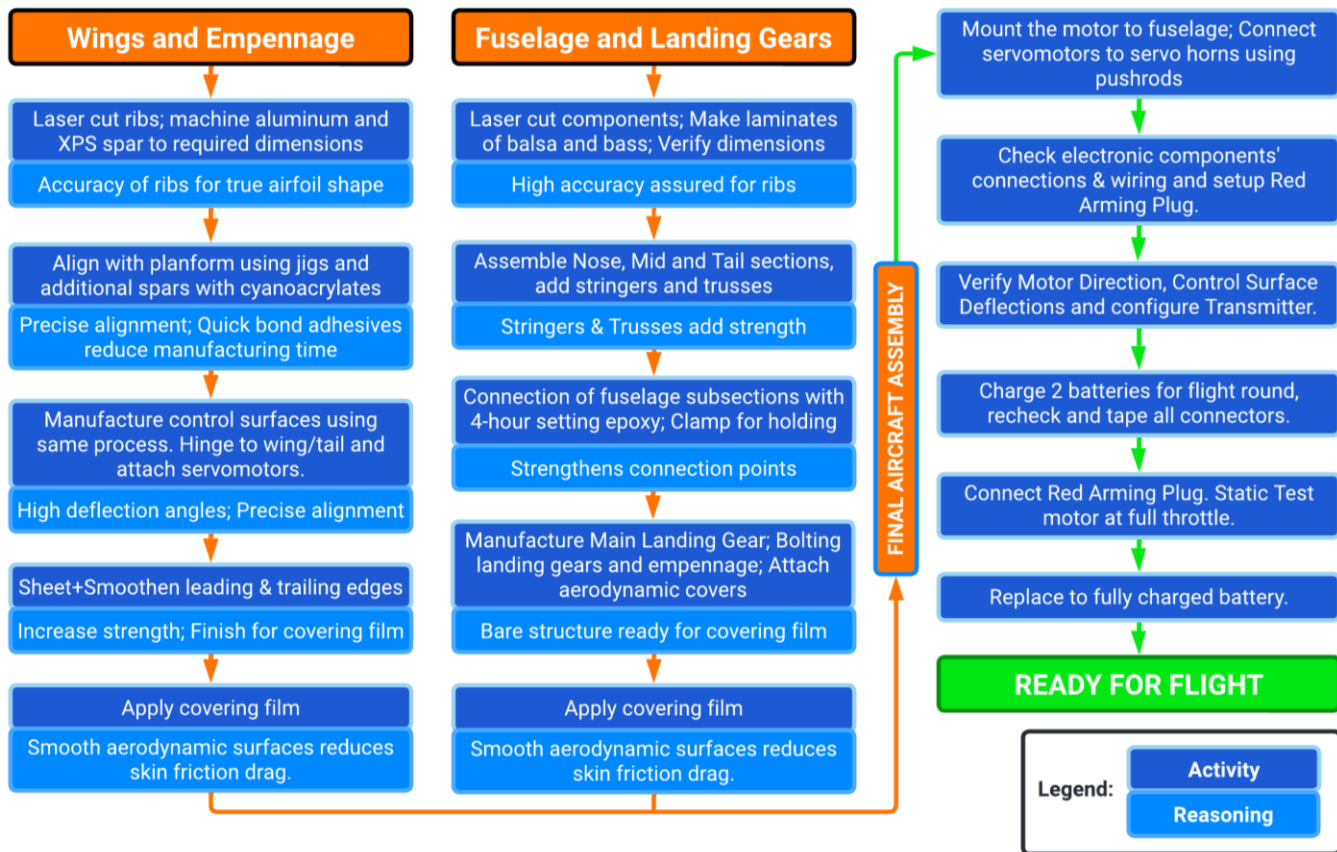


Chart 7(a): Manufacturing Process

8.0 Conclusion

The designed aircraft can carry 1 soccer ball and 17.265 lbs. of boxed cargo with the unique combinations of materials used ensuring structural soundness. Exhaustive analyses followed by extensive empirical testing validated our design. Despite the challenges faced, we hope to make the most of the opportunity and expect to be competitive at SAE Aero Design East, 2022.

Table of References:

1. Anderson, John D., "Introduction to Flight: Its Engineering and History"
2. Caughey, David A., "Introduction to Aircraft Stability and Control Course Notes"
3. Nicolai, Leland M., and Grant Carichner, "Aircraft Design"
4. Sadraey, Mohammad H., "Aircraft Design: A Systems Engineering Approach"
5. Team 019, DJS Skylark - Regular Class Design Report, SAE Aero Design Knowledge, 2021.



Appendix A – Backup Calculations

Take-off Equation: (SECTION 5.3.2)

$$S_{TO} = \frac{1}{2B} \ln \left| \frac{A}{A - BV_{TO}^2} \right| ; \text{ Where, } A = \left(\frac{T_s}{W} - \mu \right) ; \quad B = \frac{g}{\omega} \left[\frac{1}{2} \rho A (C_D - \mu C_L) + a \right] ; \quad a = 0.11126$$

Turning Radius Calculations: (SECTION 5.3.3)

$$\text{Radius} = \frac{mv^2}{L \sin \phi} ; \quad \text{Banking Angle } (\phi) = \cos^{-1} \left(\frac{W}{L} \right)$$

Servo Torque Calculations: (SECTION 6.2)

$$\text{Servo Torque Required} = (8.5 \times 10^{-6}) \frac{C^2 \times v_d^2 \times \text{control surface span} \times \sin^2(S_1)}{\cos(S_1) \times \tan(S_2)} \times \frac{\text{control horn height}}{\text{servo arm length}}$$

Aircraft Corner Speed (V^*): (SECTION 4.1.1)

$$V^* = \sqrt{\frac{2n_{max}mg}{\rho S C_{L_{max}}}} \quad n = 1 + \frac{k_g v_g E V_E \alpha \rho S}{2mg} ; \quad g = 9.80665 \text{ m/s}^2$$

Drag Polar: (SECTION 5.3.6)

$$C_D = C_{D0} + C_{Di} ; \quad C_{Di} = C_L^2 / (\pi \cdot AR \cdot e) ; \quad C_{D0} = C_{D0(\text{fuse})} + C_{D0(\text{wing})} + C_{D0(\text{Hstab})} + C_{D0(\text{Vstab})}$$

$$C_{D0(\text{surface})} = C_{f(\text{surface})} \times \text{Form Factor}_{(\text{surface})} \times \frac{\text{wetted area}}{\text{reference area}} ; \quad \text{Where, } e = \text{Efficiency Factor}$$

Climb Out: (SECTION 5.3.2)

$$\theta = \cos^{-1} \left(\frac{0.5 \rho C_L S v^2}{mg} \right) ; \quad v_y = v_x \tan \theta ; \quad v = (v_x^2 + v_y^2)^{0.5} ; \quad \text{Where, } \theta = \text{climb angle}$$

Stability Equations: (SECTION 5.3.4)

$$\text{Equilibrium condition: } C_{Mo} + C_L(h - h_o) - C_{LT} * \bar{V} = 0 ; \quad \text{Where, } C_{Mo}, C_{LT} = \text{Coefficient of moment of wing and lift of tail}$$

$$\text{For negative slope of } C_M \text{ vs } \alpha: \frac{\delta C_m}{\delta \alpha} = 0 + \frac{\delta C_L}{\delta \alpha} (h - h_o) - \frac{\delta C_{LT}}{\delta \alpha} * \bar{V}$$

$$\text{For Neutral Point: } \frac{\delta C_L}{\delta \alpha} (h_n - h_o) = \frac{\delta C_{LT}}{\delta \alpha} * \bar{V} \quad h_n = \text{Distance from Leading Edge of wing to Neutral Point}$$

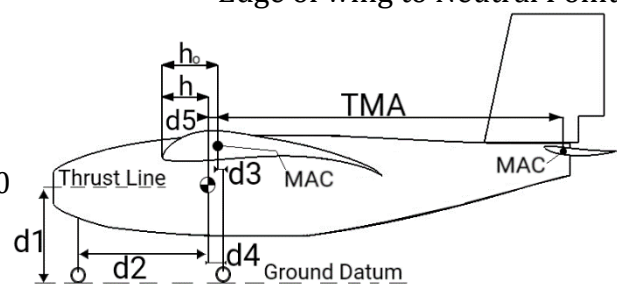
Moment Equations: (SECTION 5.3.4)

$$\text{On-ground } T_s d_1 - W d_2 \leq 0$$

$$\text{Take-off } T_d d_1 - L_{w_1} d_3 + W d_4 - L_{T_1} (TMA - d_3) = 0$$

$$\text{In flight } L_{w_2} d_5 = L_{T_2} (TMA + d_5)$$

Where,
 L_{w_1} & L_{w_2} = Lift of wing – take-off & in-flight
 L_{T_1} & L_{T_2} = Lift of Tail – take-off & in-flight





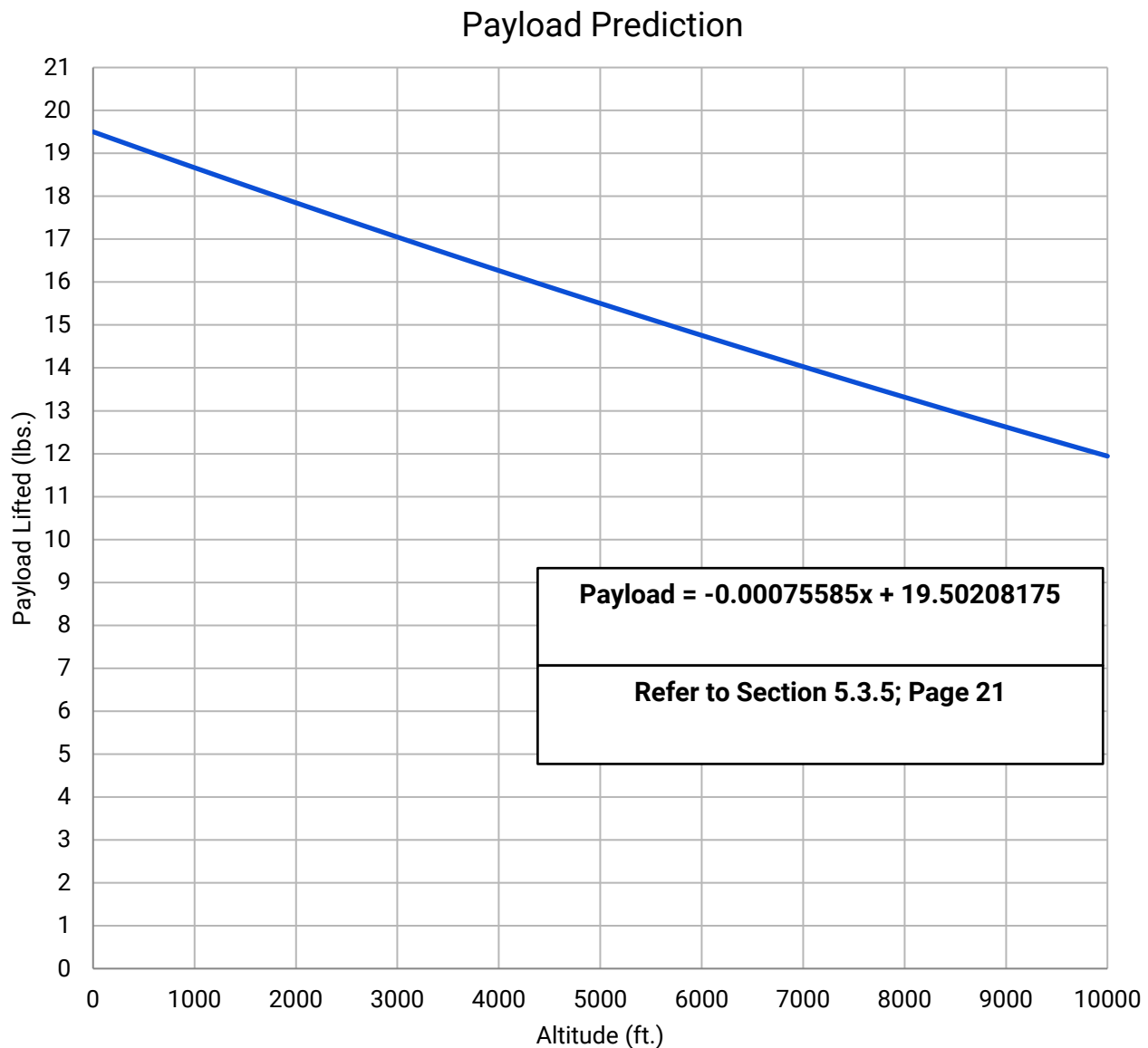
Appendix B – Technical Data Sheet

Payload Prediction Curve (Regular Class)

Team Name: DJS Skylark – Regular Class

Team Number: 026

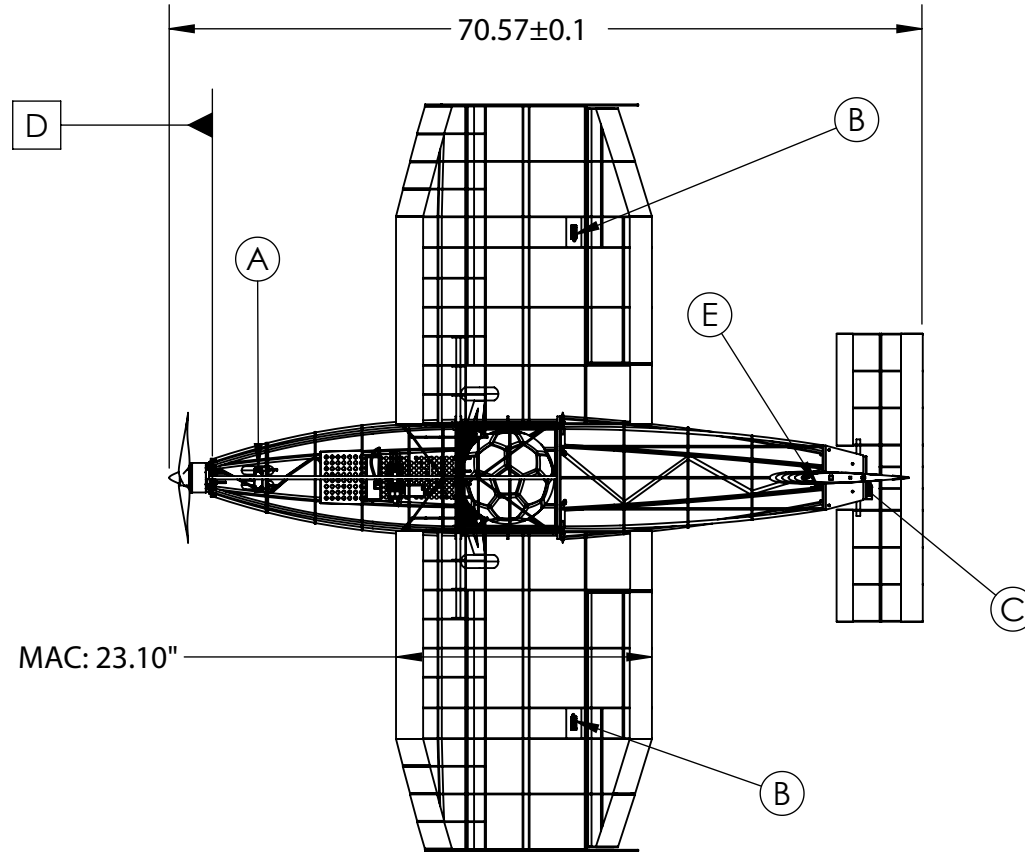
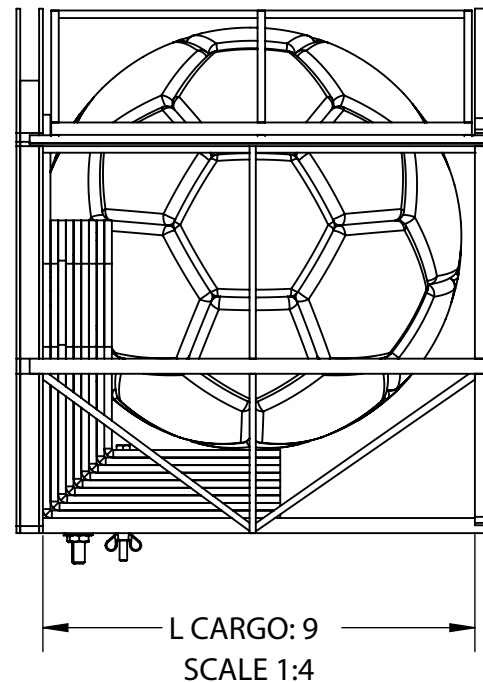
School Name: Dwarkadas J. Sanghvi College of Engineering



AIRCRAFT SUMMARY DATA

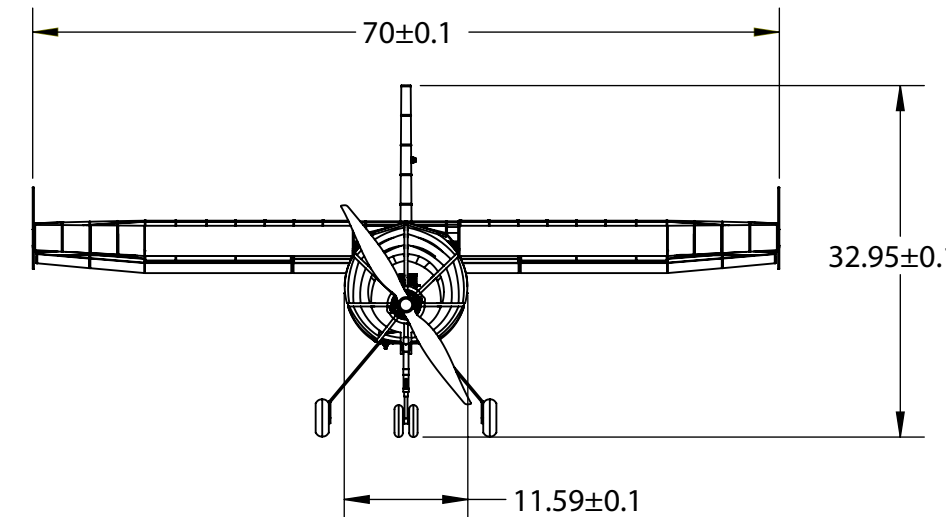
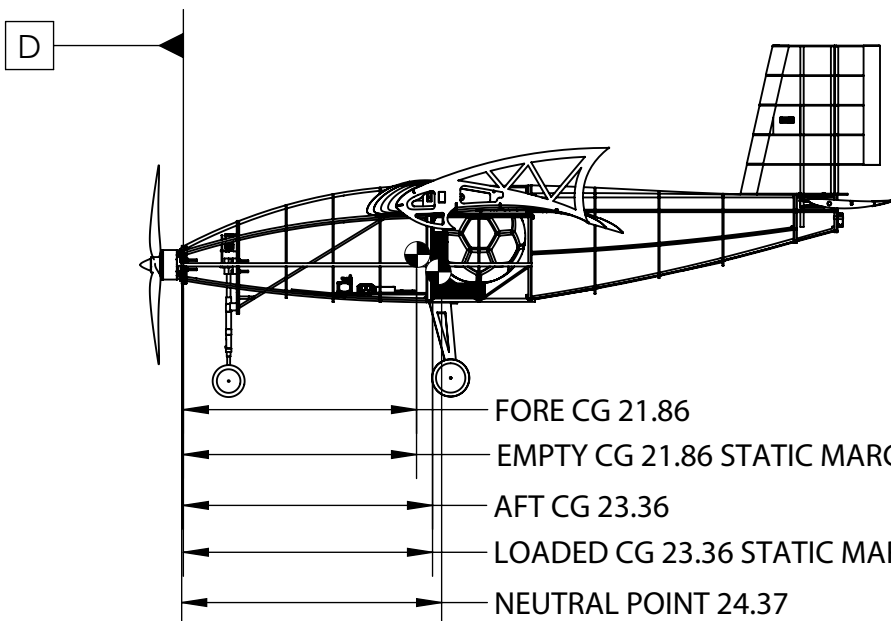
WINGSPAN	MAC	TMA	EMPTY WEIGHT	BATTERY	MOTOR MODEL	MOTOR KV	PROPELLER	SERVO (Nose Landing Gear) (A)	SERVO (Flaperon) (B)	SERVO (Stabilator) (C)	SERVO (Rudder) (E)
70 ± 0.1"	23.10"	37.5 ± 0.1"	9.4 lbs	Tattu LiPo 3300mAh 6S	SunnySky X5320-12 -14 poles	250Kv	APC 21x12WE	Turnigy TGY-WP23 (319.40oz-in)	Turnigy MX-355WP (166.64oz-in)	Turnigy TGY-WP23 (319.40oz-in)	Turnigy TGY-813 (124.99oz-in)

B

**FULLY LOADED CARGO BAY****WEIGHT & BALANCE**

SR. NO.	COMPONENTS	WEIGHT (lbs.)	ARM (in.)	MOMENT (lbs-in)
1)	MOTOR	1.124	2.00	2.248
2)	BATTERY	1.107	14.66	16.22
3)	PAYOUT	17.265	28.28	488.25
4)	ELECTRONICS	0.808	16.50	13.33
5)	SPH. CARGO	0.875	26.56	23.24

A

**BASIC DIMENSIONS**

LENGTH	$70.57 \pm 0.1"$
WIDTH	$70 \pm 0.1"$
HEIGHT	$32.59 \pm 0.1"$

Team NO: 026
Team Name: DJS Skylark - Regular Class
School Name: Dwarkadas J. Sanghvi College of Engineering
SAE Aero Design East 2022
Size: B Scale: 1:18 Unit: inches